The elemental composition of the Sun

III. The heavy elements Cu to Th[*]

Nicolas Grevesse[1,2], Pat Scott[3], Martin Asplund[4], and A. Jacques Sauval[5]

[1] Centre Spatial de Liège, Université de Liège, avenue Pré Aily, 4031 Angleur-Liège, Belgium

[2] Institut d'Astrophysique et de Géophysique, Université de Liège, Allée du 6 août, 17, B5C, 4000 Liège, Belgium
e-mail: nicolas.grevesse@ulg.ac.be

[3] Department of Physics, Imperial College London, Blackett Laboratory, Prince Consort Road, London SW7 2AZ, UK
e-mail: p.scott@imperial.ac.uk

[4] Research School of Astronomy and Astrophysics, Australian National University, Cotter Rd., Weston Creek, ACT 2611, Australia
e-mail: martin.asplund@anu.edu.au

[5] Observatoire Royal de Belgique, avenue circulaire, 3, 1180 Bruxelles, Belgium
e-mail: jacques.sauval@oma.be

ABSTRACT

We re-evaluate the abundances of the elements in the Sun from copper ($Z = 29$) to thorium ($Z = 90$). Our results are mostly based on neutral and singly-ionised lines in the solar spectrum. We use the latest 3D hydrodynamic solar model atmosphere, and in a few cases also correct for departures from local thermodynamic equilibrium (LTE) using non-LTE (NLTE) calculations performed in 1D. In order to minimise statistical and systematic uncertainties, we make stringent line selections, employ the highest-quality observational data and carefully assess oscillator strengths, hyperfine constants and isotopic separations available in the literature, for every line included in our analysis. Our results are typically in good agreement with the abundances in the most pristine meteorites, but there are some interesting exceptions. This analysis constitutes both a full exposition and a slight update of the relevant parts of the preliminary results we presented in Asplund et al. (2009, ARA&A, 47, 481), including full line lists and details of all input data that we have employed.

Key words. Sun: abundances – Sun: photosphere – Sun: granulation – line: formation – line: profiles – convection

1. Introduction

Due to the Coulomb barrier and the fact that nuclear binding energy peaks at iron, the elements beyond the Fe peak ($Z \geq 29$, i.e. Cu and heavier elements) are not produced by exothermic charged-particle fusion reactions in stable nuclear burning inside stars. Instead, most of these elements are forged by successive neutron capture followed by β-decay[1]. There are two main channels through which the isotopes of the heavy elements are produced: slow and rapid neutron capture (the *s*- and *r*-processes, respectively). The distinction between *s* and *r* depends on the neutron density, such that the timescale for β-decay is shorter (*s*-process) or longer (*r*-process) than the timescale for neutron capture. Once the neutron flux recedes, the neutron-rich isotopes from the *r*-process decay back to the valley of stability (Burbidge et al. 1957; Cameron 1957). As a result, most elements have a mixed origin, although a few isotopes and elements are produced almost exclusively by one or the other neutron-capture process (e.g. Sneden et al. 2008). Roughly half of the isotopes come primarily from the *s*-process and the other half from the *r*-process (see Table 3 in Anders & Grevesse 1989, for a full inventory). Observationally, the heavy elements show large abundance variations between stars, especially at low metallicity (e.g. Roederer et al. 2014). The *r*-process produces abundance peaks mainly at $Z \approx 32$, 54 and 78 (Ge, Xe and Pt), whereas a typical *s*-process abundance pattern has peaks at $Z \approx 38$, 56 and 82 (Sr, Ba and Pb).

The main site of the *s*-process is believed to be thermally pulsing asymptotic giant branch (AGB) stars (e.g. Sneden et al. 2008). The main neutron source in these stars is thought to be $^{13}C(\alpha,n)^{16}O$, although $^{22}Ne(\alpha,n)^{25}Mg$ can also operate, especially in more massive AGB stars (e.g. Busso et al. 2001; Karakas et al. 2012). More recently, it has been realised that the *s*-process can also be efficient in rapidly-rotating massive stars at low metallicity, through the production of primary N later converted to ^{22}Ne (Pignatari et al. 2008).

The site(s) of the *r*-process have not yet been unanimously agreed upon. Numerous possibilities have been proposed, none altogether convincing. Currently the main contenders are core-collapse supernovae (e.g. in connection with a neutrino wind, Wanajo 2013) or mergers of neutron stars with either black holes or other neutron stars (Goriely et al. 2011), but achieving the necessary neutron fluxes and entropies is challenging in either case. A handful of stars at low metallicity are strongly enriched in the *r*-process elements, with an abundance pattern remarkably similar to the *r*-process signature in the solar system, suggesting

---

[*] Tables 1–3 are available in electronic form at
http://www.aanda.org

[1] In some cases the origins may also include contributions from nuclear statistical equilibrium, proton capture or interactions with neutrinos. For example, roughly half of the solar Zn is ^{64}Zn produced in nuclear statistical equilibrium (possibly in connection with hypernovae), but the neutron-rich isotopes stem from neutron capture (e.g. Kobayashi & Nakasoto 2011).

the dominance of some universal process active throughout cosmic time (e.g. Cayrel et al. 2001; Sneden et al. 2003; Frebel et al. 2007). In a few cases, the *r*-process enhancement is so high that it has enabled the detection of radioactive elements like thorium and uranium in the stellar spectra, which has made age-dating of the nucleosynthesis sites possible (*cosmo-chronology*, Butcher 1987). Because the *r*-process elements can have a primary origin (being produced from Fe-nuclei seeds) in contrast to the secondary origin of the *s*-process elements (which require first the production of ^{13}C or ^{22}Ne nuclei as neutron sources), the *r*-process should dominate in the early Universe (Truran 1981).

A proper understanding of the nuclear processes involved in the production of the heavy elements requires a detailed knowledge of the solar system abundances. In a recent review (Asplund et al. 2009: AGSS09), we presented a summary of our redetermination of nearly all available elements in the solar photosphere. In this work (Paper III), we give detailed and homogeneous results for the elements Cu to Th, updating AGSS09 where necessary. We use the most recent 3D atmospheric model together with the best atomic and solar data. Previous papers in this series have focussed on Na – Ca (Scott et al. 2014a: Paper I) and the Fe group (Scott et al. 2014b: Paper II) with remaining elements to be dealt with in future studies. Amongst the heavy elements, so far zirconium (Ljung et al. 2006; Caffau et al. 2011a), osmium (Caffau et al. 2011b), europium (Mucciarelli et al. 2008), hafnium and thorium (Caffau et al. 2008) have been subjected to 3D solar analysis.

Section 2 describes the observations we use and how we employ them. Section 3 quickly recaps the salient details of the model atmospheres used in this series, and Sect. 4 describes the atomic data and NLTE corrections we have employed in this paper. In Sect. 5 we give our abundance results for all elements, followed by a discussion of their dependence on the chosen model atmosphere in Sect. 6. We compare our results with some previous compilations of the solar chemical composition for the heavy elements in Sect. 7, before concluding in Sect. 8.

2. Observations

We have employed the Jungfraujoch (Delbouille et al. 1973) and Kitt Peak (visual: Neckel & Labs 1984; near-infrared: Delbouille et al. 1981) disc-centre solar spectral atlases to carefully measure the equivalent widths of a large number of lines of the elements Cu to Th. Wherever possible, we have been very demanding in the quality of the lines we retained. We carefully examined the shape and full width of each line, to detect any trace of blending lines. We gave each line a weight from 1 to 3, depending on the uncertainty that we estimated for the measured equivalent width, factoring in potential pitfalls such as blends and continuum placement. We integrated observed and theoretical line profiles over the same wavelength regions when measuring the equivalent widths.

For most of the elements we used the measured equivalent widths to derive abundances with the new model atmosphere described in Sect. 3. In some cases however (Nb, rare earths, Hf, W), we instead update results obtained by other authors with spectral synthesis and the Holweger & Müller (1974) photospheric model, to account for the effect of the new 3D hydrodynamic solar model (Sect. 3). We included isotopic and hyperfine structure of lines as a series of blending features, as described in detail in Paper I, using the adopted atomic data detailed below for each relevant species (Sect. 4).

3. Solar model atmospheres and spectral line formation

We follow the same procedure as in Papers I and II. We use the new 3D, time-dependent, hydrodynamic simulation of the solar surface convection first employed in AGSS09 as a realistic model of the solar photosphere. The reader is referred to Paper I (Scott et al. 2014a) for further details of the 3D solar model. As demonstrated extensively by Pereira et al. (2013), this 3D model performs extremely well against an arsenal of key observational tests, indicating that the model is highly realistic. In particular, we note that our 3D solar model perfectly predicts the continuum centre-to-limb variation, which is a sensitive probe of the mean temperature structure in the typical line-forming region of the photosphere. The corresponding theoretical absolute intensities agree extremely well with observations as well.

For comparison, and to quantify the systematic errors of our abundance results, we have also again performed identical calculations with four different 1D models of the solar photosphere: the widely-used, hydrostatic, semi-empirical model of Holweger & Müller (1974; HM) which has been pressure-integrated to be consistent with our continuous opacities and chemical compositions, the mean 3D model ⟨3D⟩ obtained by spatially and temporally averaging the 3D model over about 45 min of solar time, the solar model from the grid of MARCS theoretical models extensively used for abundance analysis of solar-type stars (Asplund et al. 1997; Gustafsson et al. 2008), and the MISS semi-empirical model obtained from 1D LTE spectral inversion of Fe lines (Allende Prieto et al. 2001).

For all spectral line formation calculations we assumed local thermodynamic equilibrium (LTE). Non-LTE (NLTE) analyses performed in a 1D framework for the Sun exist to our knowledge only for Cu I, Zn I, Sr I, Sr II, Zr I, Zr II, Ba II, Eu II, Pb I and Th II (see below for individual references for each element). When such NLTE data are available, we correct the 3D LTE and 1D LTE results with those NLTE abundance corrections. We note that this is not fully self-consistent as the departures from LTE may be different in 3D than in 1D, indeed often depending on the particular 1D model atmosphere used. As a rule of thumb, NLTE effects are more pronounced in theoretical model atmospheres than in semi-empirical ones due to their steeper temperature gradients, a phenomenon dubbed "NLTE masking" by Rutten & Kostik (1982). For completeness, we also mention that NLTE calculations are often performed for flux spectra, but we employ disc-centre intensity spectra; NLTE effects tend to be less severe in intensity than flux because the absorption lines are formed at lower heights in intensity than in flux. As is clear from the few NLTE studies available, much work still remains to be done in this area for the heavy elements. The shortage of NLTE investigations is partially due to the relatively small number of experts in the field. For these elements however, perhaps the biggest reason for the dearth of NLTE analyses is a lack of necessary atomic data such as photo-ionisation cross-sections, transition probabilities and collisional rates for the many relevant atomic processes in what are often highly complicated atoms (Asplund 2005). NLTE calculations with incomplete model atoms and/or less precise atomic data can often be rather misleading – but so can LTE. The assumption of LTE is an extreme one, and not at all a cautious middle ground. Caution should therefore be exercised with elements lacking NLTE corrections. Fortunately, for the heavy elements, in most cases we rely on lines from the dominant ionisation stage, which typically exhibit less severe departures from LTE than minority species

(Asplund 2005); in the solar case the once-ionised species are typically in the majority.

As explained in Paper I, with a 3D solar model there is no need to invoke any micro- or macroturbulent velocities to obtain correct line broadening (Asplund et al. 2000). For all 1D models, we adopted a microturbulence of $1\,\mathrm{km\,s^{-1}}$. We carried out 3D line formation calculations for 45 snapshots from the full time sequence of the 3D solar model, spaced 1 min apart, and averaged them before carrying out the continuum normalisation.

4. Atomic data and line selection

The atomic data (transition probabilities, isotopic structure and hyperfine structure: HFS) we adopt are discussed in detail below for each element. We give our adopted lines, oscillator strengths, NLTE corrections, equivalent widths, excitation potentials and derived abundances for all elements in Table 1, and isotopic and HFS data in Table 2. We have also re-examined the ionisation energies and partition functions in detail, updating some data relative to AGSS09; this is not trivial, as even many recent analyses are still based on quite erroneous data. These data are given in Table 3. For Ho II our partition functions come from from Bord & Cowley (2002), and for all other species, from Barklem & Collet (in preparation); these are in good agreement with values computed from NIST atomic energy levels. Our ionisation energies come from the NIST data tables.

Modern line-broadening data for collisions with hydrogen atoms are available from Barklem, Piskunov & O'Mara (2000) for all the neutral lines we consider in this paper, but only Ba II and Sr II amongst the ionised lines. We use this data wherever it exists; otherwise, we use the classical recipe of Unsöld (1955) with an enhancement factor of 2.0.

4.1. Copper

Although Cu is essentially once ionised in the solar photosphere, only Cu I lines have been identified in the solar spectrum. From the works of Kock & Richter (1968) and Sneden & Crocker (1988), we retained the five Cu I lines given in Table 1. For the first three lines, we have used the experimental gf-values of Kock & Richter, renormalised to the lifetimes of Carlsson et al. (1989; the renormalisation amounts to a change of only −0.006 dex). For the last two lines, we took oscillator strengths from Bielski (1975), based on the measurements of Meggers et al. (1961).

Cu is approximately 69.2% ^{63}Cu and 30.8% ^{65}Cu (Rosman & Taylor 1998), both of which have nuclear spin $I = \frac{3}{2}$. The strongest solar lines are affected by isotopic broadening and HFS. We accounted for isotopic splitting using the data of Fischer et al. (1967). We took HFS constants from the same paper as well as from Hannaford & McDonald (1978).

NLTE Cu I line formation in the Sun was investigated by Shi et al. (2014), who found positive NLTE corrections (≈+0.02 dex) for our first three lines, and a larger negative correction (≈−0.05 dex) for the last line (Cu I 809.3 nm). We adopt their results for $S_\mathrm{H} = 0.1$, as recommended in their paper. Because the Cu I 793.3 nm and Cu I 809.3 nm lines differ only in the J values of their lower levels, and Shi et al. (2014) explain the large negative NLTE offset in the abundance returned by Cu I 809.3 nm as mainly due to underpopulation of the upper level of this transition, we assume that the NLTE correction for Cu I 793.3 nm is the same as for Cu I 809.3 nm. The addition of NLTE corrections for Cu I is a new feature of the analysis here,

compared to AGSS09. We note that the NLTE study of Shi et al. is for flux rather than disc-centre intensity spectra, which means that the adopted NLTE effects may be slightly exaggerated.

4.2. Zinc

Zinc is mostly neutral in the photosphere. We retain the five Zn I lines given in Table 1. The gf-values we use come from Biémont & Godefroid (1980a), whose theoretical results agree well with measured lifetimes. For two lines (472.2 nm and 481.0 nm), we renormalise these data to the accurate lifetimes measured by Kerkhoff et al. (1980) using laser spectroscopy, resulting in an increase of 0.01 dex.

Y. Takeda (priv. comm.) used the model atom from Takeda et al. (2005) to compute NLTE corrections of between −0.01 and −0.04 dex for our lines at the centre of the solar disc, for different values of S_H. For S_H values between 0.1 and 1 the NLTE corrections vary very little. We chose to use the corrections at $S_\mathrm{H} = 0.3$.

4.3. Gallium

Although essentially once ionised, only the near-UV Ga I resonance line at 417.2 nm (see Table 1) has been used by Ross & Aller (1970) and Lambert et al. (1969) to derive the solar Ga abundance. This line is rather heavily perturbed and can only be extracted by spectrum synthesis; doing so, these authors found $\epsilon_\mathrm{Ga} = 2.80$ and $\epsilon_\mathrm{Ga} = 2.84$ respectively. Lambert et al. also suggested using a very faint unidentified infrared line at 1194.915 nm. They argued that this line could be due to Ga I, as in their analysis it led to an abundance in agreement with the near-UV line. Oscillator strengths have been discussed by Lambert et al., and we adopt their chosen value for the near-UV line. This comes from Cunningham & Link (1967), who set a theoretical branching fraction to an absolute scale with their own accurate experimental lifetime.

We rechecked the IR line: it is suspiciously wide (suggesting unidentified blends), and its equivalent width is too inaccurate to keep as a good abundance indicator. We therefore synthesised the spectrum around the near-UV resonance line and derived an accurate estimate of the Ga I contribution: 5.22 ± 0.30 pm.

4.4. Germanium

Ge is also mostly once ionised in the solar photosphere, but only very few Ge I lines have been identified. Accurate gf-values have been measured by Biémont et al. (1999). With the only usable Ge I line (326.9 nm; Table 1), they applied their oscillator strength to derive a solar abundance of $\log \epsilon_\mathrm{Ge} = 3.58$.

We also investigated the intercombination line at 468.583 nm suggested by Lambert et al. (1969) as a possible indicator of the Ge abundance. It is however blended by a Co I line, which contributes 0.155 pm to the total equivalent width of the feature when computed with the new solar Co abundance derived in Paper II. With this blend removed, the equivalent width is about 0.4 pm, and the abundance of Ge derived from this line is about a factor of four too large; this line is definitely blended by another unknown line.

4.5. Arsenic

No As line is definitively identified in the solar spectrum. Gopka et al. (2001) used two lines in the near-UV, at 299.0984 and

303.2846 nm, believed to be due to As I to derive the solar abundance of As. They found $\log \epsilon_{As} = 2.33$, although the gf-values for these two As I lines are extremely uncertain. As explained below, we argue that no reliable As abundance can be derived for the Sun with the available information.

4.6. Rubidium

Rubidium is very much once-ionised in the solar photosphere, but only two faint, near-IR resonance lines of Rb I at 780.0 and 794.7 nm can be identified (Table 1). Both are strongly broadened by isotopic and hyperfine structure, and perturbed by stronger neighbouring lines (e.g. the 794.7 nm line is heavily perturbed by a water vapour line). We very carefully measured the equivalent widths of the two Rb I lines, eventually using spectral synthesis to derive the best values. We measured the faintest line only on the Jungfraujoch solar spectrum, which shows by far the smallest water vapour content of the available solar atlases.

Accurate gf-values are available for both lines, from lifetime measurements of the upper levels by Volz & Schmoranzer (1996) and Simsarian et al. (1998). As advocated by Morton 2000), we adopted the mean from these two studies, weighted according to their uncertainties.

Natural Rb shows HFS because it is about 72.2% ^{85}Rb, with $I = 5/2$, and 27.8% ^{87}Rb, with $I = 3/2$ (Rosman & Taylor 1998). We took HFS constants from a range of different sources. For ^{85}Rb, we adopted values from Nez et al. (1993), Rapol et al. (2003) and Beacham & Andrew (1971). We used data from Beacham & Andrew also for ^{87}Rb, as well as from Ye et al. (1996) and Bize et al. (1999). Isotopic splitting in these lines is small compared to the separation of HFS components (Banerjee et al. 2004) and thus neglected here.

Relative to AGSS09, in this analysis we have added HFS data and updated the oscillator strengths for both lines.

4.7. Strontium

We analysed the few Sr I and Sr II lines previously studied by Gratton & Sneden (1994) and Barklem & O'Mara (2000), listed in Table 1. These authors also discuss the accuracy of available gf-values in detail. For the two Sr I lines, we adopted experimental oscillator strengths from García & Campos (1988), who normalised their own relative values using existing accurate lifetimes, and Migdalek & Baylis (1987). For Sr II, we derived gf-values by setting the relative data of Gallagher (1967) to an absolute scale using the mean of lifetimes from Kuske et al. (1978) and Pinnington et al. (1995). The Sr I gf-values are substantially more precise overall (±0.02–0.03 dex) than the Sr II ones (±0.08 dex).

The broadening parameters for the rather strong IR lines of Sr II have been calculated by Barklem & O'Mara (2000).

We treat each Sr line as a single component in our abundance calculations, as isotopic splitting is small for Sr lines (Hauge 1972b), and HFS exists only for ^{87}Sr (which accounts for just 7% of Sr).

M. Bergemann (priv. comm.) has computed NLTE corrections for disc-centre intensity both for our Sr I and Sr II lines at $S_H = 0.05$ using the MARCS, HM and ⟨3D⟩ models; for the 3D case we adopt the ⟨3D⟩ results, which should closely approximate the full 3D results. The NLTE effects are substantial, and in opposite directions for Sr I and Sr II (Table 1). Bergemann's

results are in good agreement with those of Mashonkina & Gehren (2001) for the three Sr II lines.

Relative to AGSS09, we have updated the NLTE corrections and the gf-value of the Sr I 707.0 nm line. We also discarded the Sr II line at 416.1 nm, because no accurate gf-value is available for this line.

4.8. Yttrium

The most recent solar analysis is from Hannaford et al. (1982). They obtained accurate gf-values, both for Y I and Y II lines, combining lifetimes with branching fraction measurements. They derived the solar abundance of Y, $\log \epsilon_Y = 2.24 \pm 0.03$ from eight Y I and 41 Y II solar lines. In the present work we carefully examined all these solar lines, deciding to discard all Y I lines because they are very weak, with large uncertainties arising from the measurement of equivalent widths. Adopting the same demanding selection criteria as for other elements, we reduced the Y II sample to the ten best lines. We adopted gf-values from Hannaford et al. (1982) directly for seven of these. For the other three (490.0, 547.3 and 572.8 nm), we updated the gf-values of Hannaford et al. using new accurate lifetimes by Wännström et al. (1988) and Biémont et al. (2011). We calculated new lifetimes as means of lifetimes from as many of these three sources as possible in each case. We took unweighted means, as differences between the three sets of lifetimes indicate a systematic error that is not quantified in any of the stated lifetime errors.

Y consists entirely of ^{89}Y, which has $I = \frac{1}{2}$. We included HFS data for Y II lines where available, drawing on HFS constants measured by Wännström et al. (1988) and Dinneen et al. (1991), as well as theoretical calculations by Beck (1992).

Relative to AGSS09, we have added HFS data for all lines, and renormalised the oscillator strengths of the 490.0, 547.3 and 572.8 nm lines.

4.9. Zirconium

Zr is essentially in the form of Zr II in the solar photosphere. However, a large number of faint Zr I lines are also present in the photospheric spectrum. Biémont et al. (1981) measured gf-values by the lifetime+branching fraction technique for a large number of Zr I and Zr II transitions, and applied these data to determine the solar abundance of Zr, using equivalent widths and the HM model. Thirty-four Zr I and 24 Zr II lines led to the same result (Zr I: $\log \epsilon_{Zr} = 2.57 \pm 0.21$, Zr II: $\log \epsilon_{Zr} = 2.56 \pm 0.14$), but the dispersions are uncomfortably large. This indicates that many solar Zr I and Zr II lines are blended. Ljung et al. (2006) measured new branching fractions and combined them with previously-measured lifetimes to obtain a new set of accurate Zr II gf-values. These authors also analysed a few solar Zr II lines, using their new data, equivalent widths and an older version of the 3D model that we employ in this series (they used the same model as used in AGS05) to derive a 3D LTE solar abundance of $\log \epsilon_{Zr} = 2.58 \pm 0.02$ (standard deviation).

As for other elements, we carefully selected the lines to be used in the present abundance analysis. Although we give Zr I results for comparison in Tables 1 and 4, using oscillator strengths from Biémont et al. (1981), we do not retain Zr I as a good indicator of the solar Zr abundance. This is because the lines are all very weak and many are blended. Because Zr I is the minor species, it is also prone to very large departures from LTE ($\approx +0.3$ dex for $S_H = 1.0$), whereas low excitation Zr II lines are essentially formed in LTE (Velichko et al. 2010); note though

that Velichko et al. (2011) suspect that their published NLTE corrections are overestimated due to their incomplete Zr I model atom. We finally retained the ten low-excitation Zr II lines given in Table 1. The gf-values are mean values (on a log scale) from Biémont et al. (1981) and Ljung et al. (2006), except for 402.4 nm, which comes only from Ljung et al., as it was not measured by Biémont et al. For our lines, the differences between these two data sets are within the claimed uncertainties, and the uncertainties of the mean gf-values we adopt are of order 5−10%.

4.10. Niobium

Because of the rather large ratio Nb II/Nb I, as discussed in Hannaford et al. (1985), only Nb II is a reliable indicator of the solar abundance of Nb. All useful Nb II lines are unfortunately strongly blended in the solar photospheric spectrum. We therefore choose to update the recent value obtained by Nilsson et al. (2010), who derived the solar Nb abundance from spectral synthesis using the HM model. They used accurate new experimental gf-values and HFS data from Nilsson & Ivarsson (2008), supplemented by some of their own oscillator strengths. We adopt the same data here. Nb is entirely ^{93}Nb ($I = \frac{9}{2}$), so HFS is important but isotopic structure is not.

In AGSS09 we performed our own analysis without HFS, whereas here we update the result of Nilsson et al. (2010), using HFS data.

4.11. Molybdenum

Mo is essentially once ionised in the solar photosphere. Unfortunately all the lines identified as Mo II are too blended to be useful, except for one at 329.2 nm. However, no gf-value exist for this line apart from the value from Corliss & Bozman (1962), which suffer from large uncertainties. The abundance result from this Mo II line appears to be orders of magnitude larger than the meteoritic value, indicating a problem with the transition probability. We therefore rely on the minor indicator, Mo I, as done by Biémont et al. (1983). They used accurate gf-values from Whaling et al. (1984), finding $\log \epsilon_{\mathrm{Mo}} = 1.92 \pm 0.05$ with twelve very faint lines, all difficult to measure. After a careful analysis of these lines, we retain just two as reliable indicators of the Mo abundance (Table 1). For these lines, we employ the slightly improved oscillator strengths of Whaling & Brault (1988).

Mo consists of a pot pouri of different isotopes, but the two lines we use are very weak, and their isotopic splitting is small (Hughes 1961; Golovin & Striganov 1968). We can therefore safely ignore isotopic and hyperfine structure for these lines.

Compared to AGSS09, we use the gf-values of Whaling & Brault (1988) instead of those of Whaling et al. (1984), which translates to a mean abundance change of −0.02 dex.

4.12. Ruthenium

As for the previous elements, the ratio Ru II/Ru I is large in the solar photosphere. Unfortunately none of the Ru II lines identified in the solar spectrum could be used as they are all hopelessly blended. New gf values have recently been measured and computed by Fivet et al. (2009) for a large number of lines of Ru I. These new data are in reasonable agreement with the accurate gf-values measured by Wickliffe et al. (1994) using the lifetime+branching fraction technique. We rely on the purely

experimental gf-values rather than using the data from Fivet et al. (2009), because for our lines, the latter are based only on theoretical values.

Fivet et al. (2009) applied their new data to determine the solar Ru abundance from six good Ru I lines: $\log \epsilon_{\mathrm{Ru}} = 1.72 \pm 0.12$. We adopt the same six lines in our analysis (Table 1). Whilst Ru consists of many different isotopes, the only isotopic splits available are for the 408.1 nm and 455.5 nm lines, which are so weak that isotopic structure has no effect for abundance determinations.

Relative to AGSS09, here we use gf-values from Wickliffe et al. (1994) instead of Fivet et al. (2009).

4.13. Rhodium

The ratio Rh II/Rh I is again large in the solar photosphere. Unfortunately, none of the few Rh II lines identified in the UV can be measured: they are all very heavily blended and could not be analysed even by spectrum synthesis. Kwiatkowski et al. (1982) measured lifetimes for Rh I and derived gf-values by combining these lifetimes with branching fractions from Corliss & Bozman (1962). They used these new gf-values with the HM model and a sample of solar Rh I lines in the near UV, to derive an abundance of $\log \epsilon_{\mathrm{Rh}} = 1.12 \pm 0.12$. As many of these lines are quite difficult to measure with accuracy, we only retain two of them as reliable indicators of the Rh abundance. We adopt the gf-values of Kwiatkowski et al. (1982) for both these lines, as later data (Duquette & Lawler 1985) suffers from radiation trapping for the only one of our lines measured.

Rhodium is 100% ^{103}Rh, which has nuclear spin $I = \frac{1}{2}$. Where possible, we include HFS data for our two lines, from Chan et al. (1968). The analysis in AGSS09 did not include HFS.

4.14. Palladium

The ratio Pd II/Pd I is about 4 in the solar photosphere but no Pd II lines have been identified in the solar spectrum. The most recent Pd abundance is from Xu et al. (2006), who combined new lifetimes and branching fractions to derive accurate gf-values for Pd I lines. They used these new data to refine an earlier analysis by Biémont et al. (1982), using equivalent widths, five of the eight Pd I lines employed in the earlier study, and the same HM model. As the lines are very perturbed, we only retain two of those used in these earlier works.

Isotopic and hyperfine structure is small for Pd I (Engleman et al. 1998) and can be ignored for our purposes.

4.15. Silver

There is no Ag II line in the solar spectrum. The only two Ag I lines are in the near-UV (see Table 1), and very difficult to measure because of blends and uncertainty in the continuum placement. Grevesse (1984) revised an older analysis by Ross & Aller (1972; $\log \epsilon_{\mathrm{Ag}} = 0.85 \pm 0.15$), using gf-values from Hannaford & Lowe (1983). We adopt newer gf-values here, based on the total lifetime of the resonance doublet as measured by Carlsson et al. (1990), and the relative contribution of each line calculated by Civiš et al. (2010).

Silver is approximately 51.8% ^{107}Ag and 48.2% ^{109}Ag (both $I = \frac{1}{2}$), and exhibits substantial isotopic and hyperfine structure. We calculated the isotopic separations of our Ag I lines using data from Crawford et al. (1949) and Jackson & Kuhn (1937), relying on component identifications from Brix et al. (1951) and

Wessel & Lew ([1953](#)). We took HFS constants from the experiments of Wessel & Lew ([1953](#)) and Carlsson et al. ([1990](#)).

Compared to AGSS09, here we employ both updated HFS data and oscillator strengths; in AGSS09 we used the gf-values of Hannaford & Lowe ([1983](#)).

4.16. Cadmium

There is a Cd I line identified in the solar spectrum at 326.1065 nm, but it is awfully blended. Even spectrum synthesis by Youssef et al. ([1990](#)) was not very successful; we have chosen to discard this line. Another line (508.6 nm; Table [1](#)) was attributed to Cd I by Lambert et al. ([1969](#)). Youssef et al. derived the Cd abundance from this very weak line using the HM model and an accurate gf-value, measured by the lifetime+branching fraction technique by Veer et al. ([1990](#)). We adopt this line and the same oscillator strength for our analysis.

We carefully measured the 508.6 nm line, finding an equivalent width of 0.100 ± 0.015 pm. This line is however also blended, by a faint Fe I line. The lower level of the Fe I line has an excitation energy of 3.88 eV, but the line has no accurately-known oscillator strength. The only gf-value available comes from the calculations of Kurucz ([1998](#); $\log gf = -4.325$); the accuracies of Kurucz's semi-empirical gf-values degrade markedly as one moves to weaker transitions such as this. In order to empirically estimate the contribution of this blend, we identified five other weak Fe I lines with similar excitation potentials, near to the 508.6 nm line in wavelength. We measured their equivalent widths, and used the Fe abundance derived in Paper II together with the relative gf-values to estimate the equivalent width of the Fe I contribution to the feature at 508.6 nm. We found an implied Fe I equivalent width of 0.027 ± 0.014 pm, giving an overall Cd I contribution of 0.073 ± 0.021 pm.

4.17. Indium

Although indium is essentially In II because of its very low ionisation energy (5.78 eV; the ratio In II/In I is >100 in the solar photosphere), there is only one identified In I line in the solar photospheric spectrum, at 451.13 nm. This line has been analysed by many authors: Lambert et al. ([1969](#)), Bord & Cowley ([2001](#), [2002](#)) and Gonzalez ([2006](#)). Their results for the solar abundance of indium cluster around $\log \epsilon_{\mathrm{In}} = 1.60$, which is 0.84 dex larger than the meteoritic value: $\log \epsilon_{\mathrm{In}} = 0.76 \pm 0.03$ (Lodders et al. [2009](#)). To explain this large difference, Bord & Cowley and Gonzalez suggested that because its condensation temperature is just 536 K, indium did not fully condense in the solar nebula, leading to a relative depletion in meteorites. However, other elements with similarly low condensation temperatures do not exhibit the same differences in their solar and meteoritic abundances.

Vitas et al. ([2008](#)) recently made a detailed analysis of this In I line by spectrum synthesis, including HFS and many known blends. They concluded that the photospheric line at 451.13 nm is in fact not In I, because they could not reproduce the observed spectrum, regardless of their adopted indium abundance. They also analysed the same region in a sunspot spectrum, finding that it could be reproduced nicely by spectrum synthesis with the meteoritic indium abundance, if Zeeman splittings were properly taken into account. Vitas et al. therefore suggest that the solar indium abundance is the meteoritic value, and that the photospheric line at 451.13 nm is due to an unidentified

high-excitation ionic line, which disappears in the much cooler sunspot.

Based on the ratio Sn/In, Vitas et al. ([2008](#)) also make the argument that the observed meteoritic ratio is perfectly reproduced by models of r- and s-process nucleosynthesis, but that the high solar In abundance is not.

4.18. Tin

The ratio Sn II/Sn I is about 10. The only reasonable Sn line available is a very weak Sn I line in the near-UV (see Table [1](#)). We adopt the gf-value obtained by Lotrian et al. ([1976](#)) for this line, from lifetime and branching fraction measurements. The equivalent width of this very faint line (0.12 pm) has an uncertainty of order 20%, i.e. 0.08 dex. Although tin has many significant isotopes, for this line isotopic structure is neither available nor, given its weakness, necessary.

4.19. Antimony

Only one very faint and perturbed line has been identified as Sb I in the solar photospheric spectrum, at 323.2547 nm. The abundance of Sb has not been re-analysed for many decades: the latest result was from Grevesse et al. ([1968](#)), slightly revised by Ross & Aller ([1976](#)) to $\log \epsilon_{\mathrm{Sb}} = 1.00$. This value had a very large uncertainty, difficult to estimate because of the uncertainty of the equivalent width and the fact that the only available gf-value came from the notoriously uncertain data of Corliss & Bozman ([1962](#)). We measured an equivalent width of 0.045 ± 0.015 pm, with a large uncertainty of 33%. Spectral synthesis would not substantially reduce this error, given how weak and badly blended this line is.

Guern & Lotrian ([1980](#)) and Gonzales et al. ([1997](#)) measured the oscillator strength of this line by combining lifetimes and branching fractions, but the values differ by 0.18 dex: $\log gf = -0.72$ and -0.90, respectively.

4.20. Barium

Because of its low ionisation energy, Ba is essentially Ba II in the photosphere. We retained the three Ba II lines of Table [1](#). These lines are sensitive to NLTE effects, and substantially broadened by HFS. M. Bergemann (priv. comm.) computed the NLTE effects for these lines. Her values at $S_{\mathrm{H}} = 0.05$ (Table [1](#)) are in excellent agreement with the results of Mashonkina et al. ([1999](#)) and Mashonkina & Gehren ([2000](#)). We adopt the accurate gf-values available from Davidson et al. ([1992](#)) and Kurz et al. ([2008](#)).

The many stable isotopes of Ba are present in the approximate ratio $^{130}\mathrm{Ba}$:$^{132}\mathrm{Ba}$:$^{134}\mathrm{Ba}$:$^{135}\mathrm{Ba}$:$^{136}\mathrm{Ba}$:$^{137}\mathrm{Ba}$:$^{138}\mathrm{Ba} = 0.1$:0.1:2.4:6.6:7.9:11.2:71.7 (Rosman & Taylor [1998](#)), with only the odd-A nuclei possessing nuclear spin ($I = \frac{3}{2}$ in both cases). We obtained isotopic separations for the 455.4 nm line from Wendt et al. ([1984](#)), from van Hove et al. ([1982](#)) for the 585.4 nm line, and from Villemoes et al. ([1993](#)) for the 649.7 nm line. We also drew on the latter for HFS data, along with the papers of Trapp et al. ([2000](#)) and van Hove et al. ([1985](#)).

In AGSS09 we did not include the 455.4 nm line. Here we have also updated the HFS, isotopic and NLTE data, as well as the oscillator strength of the 585.4 nm line.

4.21. Rare Earths (La to Lu) and Hafnium

In recent years, the Wisconsin group have systematically measured the atomic data required for accurate abundance analyses of all the once-ionised species of the rare Earth elements. They have derived accurate gf-values by measuring lifetimes and branching fractions, as well as HFS constants and isotopic splits wherever necessary. With the HM model, spectral synthesis and/or equivalent widths, and as many lines as possible, they have systematically applied their very accurate atomic data to the determination of the solar abundances of all the rare Earth elements (La: Lawler et al. 2001a, Ce: Lawler et al. 2009, Nd: Den Hartog et al. 2003, Sm: Lawler et al. 2006, Eu: Lawler et al. 2001b, Gd: Den Hartog et al. 2006, Tb: Lawler et al. 2001c, Ho: Lawler et al. 2004, Er: Lawler et al. 2008), Pr, Dy, Tm, Yb, and Lu: Sneden et al. 2009), as well as Hf (Lawler et al. 2007).

We have not repeated the careful spectral synthesis computations done by Sneden, Lawler and collaborators, but rather corrected them for the abundance differences we see between the results with our 3D model and the HM model. For this purpose we have selected a sample of representative lines of each species, and have derived the 3D-HM abundance differences. We included all HFS and isotopic splittings summarised by Sneden et al. (2009) in our calculations.

For Nd, new gf-values are also available from Li et al. (2007). Taking the mean of gf-values from Li et al. (2007) and from Den Hartog et al. (2003) produces exactly the same abundance as using only the values of Den Hartog et al, however.

For Sm II, new accurate gf-values have been measured by Rehse et al. (2006), which agree quite well with the values of Lawler et al. (2006). We chose to adopt the mean of the gf-values from these two sources. In AGSS09 we simply adopted the values of Lawler et al. (2006).

As in the analysis of AGSS09, for Eu we also applied a small NLTE correction of +0.03 dex for every line, as derived by Mashonkina & Gehren (2000). We are not aware of any other NLTE study of rare Earth elements in the Sun.

For Tb II, we only kept one of the three lines (365.9 nm) used by Lawler et al. (2001c), because of the difficulty in fitting the profiles of the other two, due to blends and very wide HFS.

4.22. Tungsten

The ratio W II/W I is of order ten in the solar photosphere but unfortunately no W II lines are available in the solar spectrum. Holweger & Werner (1982) used spectral synthesis to analyse the two weak W I lines at 400.9 and 484.4 nm with the HM model. New gf-values have become available from den Hartog et al. (1987) for both lines, and from Kling & Koch (1999) for the 484.4 nm line. Here we update the results of Holweger & Werner for the new gf-values (where we take the mean of the two new values for the 484.4 nm line); we did not previously apply this update in AGSS09.

The lines are too faint for isotopic or hyperfine structure to matter. This is in fact true of all lines we use from elements heavier than Hf, so we will discuss neither HFS nor isotopic effects any further in this Section.

4.23. Osmium

Only very few faint lines of Os I have been identified in the solar spectrum. Kwiatkowsky et al. (1984) measured accurate lifetimes and used branching fractions from Corliss & Bozman (1962) to derive gf-values for a few Os I lines of solar interest.

Quinet et al. (2006) recently made new measurements of lifetimes and combined them with modern theoretical branching fractions, leading to values in good agreement with those of Kwiatkowsky et al. (1984).

Kwiatkowsky et al. (1984) used a series of nine Os I lines to derive the solar abundance. Quinet et al. (2006) however showed that many of these lines are too faint and blended to be reliably measured. We agree with Quinet et al. (2006) that very few Os I lines are realistically usable (see their Table 7). We are ultimately even more demanding than them in our line selection: we only retain the 330.2 nm line as the unique tracer of the solar Os abundance. We adopt the accurate experimental oscillator strength of Ivarsson et al. (2003) for this line, but note that the value differs from that of Quinet et al. (2006) by only 0.003 dex. The two other lines considered by Quinet et al. (327.0 and 442.0 nm; see their Fig. 6), are very difficult to analyse accurately, even by spectral synthesis.

4.24. Iridium

Drake & Aller (1976) analysed the Ir I line at 322.1 nm by spectrum synthesis. Youssef & Khalil (1988) analysed three Ir I lines in the near-UV, including the 322.1 nm line, also by spectrum synthesis using the HM model.

We retain only the 322.1 nm Ir I line, as the other two used by Youssef & Khalil (1988) are too heavily perturbed. Even the 322.1 nm line is itself heavily blended. Rechecking this line in the Jungfraujoch solar tracing (Delbouille et al. 1973; no tracing is available from Kitt Peak at these wavelengths) we noticed that Youssef & Khalil's adopted continuum was too high in this spectral region. We therefore directly remeasured the equivalent width of this blended line: 0.975 ± 0.125 pm. We confirmed this value using spectral synthesis with the HM solar photospheric model.

We have been able to derive a very accurate gf-value for 322.1 nm line, using lifetime measurements by Gough et al. (1983; uncertainty 3.6%) and Xu et al. (2007; uncertainty 6.8%). We weighted these lifetimes by their respective uncertainties and took the mean, then paired the resulting value with the branching fraction measured by Gough et al. We did not use the theoretical branching fraction of Xu et al. because of its uncertain accuracy.

4.25. Gold

Youssef (1986) used spectral synthesis with the HM model to analyse the much-perturbed Au I 312.3 nm line (Table 1), the only useful Au feature in the solar spectrum. We carefully remeasured this Au I line on the Jungfraujoch disc-centre solar spectrum (Delbouille et al. 1973); no Kitt Peak spectrum is available in this wavelength region. We found an equivalent width of 0.29 pm, with an uncertainty of 10%.

A very weak Fe I line is known to exist coincident with the Au I line, with parameters $\lambda = 312.2775$ nm, $E_{exc} = 2.45$ eV, $\log gf = -4.144$ (Kurucz 1998). Unfortunately, the oscillator strength is not reliable enough to make any serious estimate of the contribution to the equivalent width of the Au I line, and the spectrum is far too crowded in this region to employ the same strategy as we did for Cd I, where we relied on a number of other nearby faint Fe I lines.

The best available gf-value for the Au I line comes from Hannaford et al. (1981), who obtained $\log gf = -0.95 \pm 0.06$ with lifetime and branching fraction measurements. The lifetime

of Hannaford et al. for the upper level agrees perfectly with that obtained by Gaarde et al. ([1994](#)) using a similar technique.

4.26. Lead

Biémont et al. ([2000](#)) used one Pb I line, for which they had accurately derived the gf-value, to revise the solar Pb abundance. We use the same line and oscillator strength (Table [1](#)), but our equivalent width is 0.855 ± 0.035 pm instead of 0.91 pm, derived anew for this paper by both direct measurement and spectrum synthesis. This line is situated in the outer red wing of an extremely strong line with contributions from Co I, Fe I and V I, and in the outer blue wing of a somewhat less strong Fe I line. The continuum is very difficult to determine in this crowded region, but a viable reference point can be found at 3683.8 Å. We rule out the large equivalent width of Biémont et al.; our spectral synthesis calculations confirm that their continuum placement is incorrect.

Mashonkina et al. ([2012](#)) computed the effect of departures from LTE on the formation of this Pb I line at the centre of the solar disc, which are substantial. Between $S_H = 0$ and $S_H = 1$, the NLTE correction with the MARCS model atmosphere varies from $+0.15$ to $+0.07$ dex. We adopt Mashonkina et al.'s preferred value of $+0.12$ dex, derived with $S_H = 0.1$. At the time of AGSS09, no NLTE correction was available.

4.27. Thorium

The only reliable faint Th II line lies at 401.9 nm, in the red wing of a much stronger Fe I line. It is also blended by Co I and V I lines, both with about the same wavelengths.

The best oscillator strength for the Th II line comes from the accurate lifetime+branching fraction results of Nilsson et al. ([2002](#)). Atomic data (wavelengths, HFS and gf-values) concerning the blends are known from the works of Learner et al. ([1991](#)), Lawler et al. ([1990](#)) and Pickering & Semeniuk ([1995](#)). Although the gf-value for the Co I line ($\log gf = -2.27 \pm 0.04$, $E_{exc} = 2.28$ eV) is very accurate (Lawler et al. [1990](#)), the value for the V I blend ($E_{exc} = 1.80$ eV) is probably less well known, even though Pickering & Semeniuk give $\log gf = -1.30 \pm 0.04$. The stated uncertainty is for the relative value with respect to the gf-values of two stronger V I lines, to which Pickering & Semeniuk compared this line. The absolute gf-values of these stronger lines come from from Kurucz ([1998](#)), and are only known to about ± 0.08 dex.

We measured the total equivalent width of the feature containing Th II. We also computed the contributions of the Co I and V I blends from the gf-values above, and the abundances derived in Paper II, employing a number of different solar photospheric model atmospheres. The equivalent widths of the two blends predicted in this way are almost model-independent. We found predicted equivalent widths of 0.208 pm for the Co I blend, and 0.038 pm for the V I blend. As the total measured equivalent width is 0.56 pm, this leaves 0.314 pm for Th II. We estimate the uncertainty of the Th II contribution to be of order 20%, based on the uncertainty of the total measured equivalent width and the uncertainties of the Co I and V I contributions.

Mashonkina et al. ([2012](#)) estimated small NLTE corrections of between $+0.06$ dex ($S_H = 0$) and 0.00 dex ($S_H = 1$) for this Th II line, using the MARCS model atmosphere. We adopt $\Delta_{\mathrm{NLTE}} = +0.01$ dex, corresponding to $S_H = 0.1$ (Mashonkina et al.'s preferred value). This NLTE correction was not available for AGSS09.

5. Derived solar elemental abundances

The detailed results for the different model atmospheres we used are presented in Table [1](#), with each element individually discussed below. Line profiles produced in 3D generally show very good agreement with the observed spectrum; some examples are given in Fig. [1](#).

Besides statistical errors in our derived abundances (which we specify as the standard deviation of the mean), we quantify three possible systematic errors arising from potential problems in the atmospheric and atomic modelling: departures from LTE, the mean photospheric temperature structure and atmospheric inhomogeneities. We add these in quadrature to the statistical errors to estimate overall uncertainties. Full details can be found in Paper I.

In the following we compare our derived abundances to CI chondritic abundances taken from the recent careful compilation and analysis of Lodders et al. ([2009](#)). As we did in AGSS09, we renormalise these data to the photospheric abundance of silicon determined in Paper I ($\log \epsilon_{\mathrm{Si}} = 7.51$).

Below we often refer to the "3D effect" on the derived elemental abundances. We define this 3D effect as $\log \epsilon_{\mathrm{3D}} - \log \epsilon_{\mathrm{HM}}$, i.e. the correction to bring the abundance computed with the HM model into agreement with the abundance obtained with our 3D model. Although this is not strictly just the effect of using a 3D model atmosphere rather than a 1D one (see Sect. [6](#) for a discussion), we use this definition because the HM model has been the de facto standard for abundance determinations in past decades. We note that other authors prefer to define the 3D effect as $\log \epsilon_{\mathrm{3D}} - \log \epsilon_{\langle \mathrm{3D} \rangle}$ to isolate the impact of the atmospheric inhomogeneities. We argue however that differences in the mean stratification arising from the treatment of convection should be considered when evaluating the full impact of using 3D models rather than 1D ones.

5.1. Copper

Our 3D+NLTE copper abundance is

$$\log \epsilon_{\mathrm{Cu}} = 4.18 \pm 0.05 \ (\pm 0.02 \text{ stat}, \ \pm 0.04 \text{ sys}).$$

The 3D effect on these lines is rather small; with the HM model the abundance is 4.21. Interestingly, accounting for departures from LTE as computed by Shi et al. ([2014](#)) slightly increases the line-to-line scatter ($\sigma = 0.03$ and 0.05 dex, respectively) but the net effect on the Cu abundance is small (-0.01 dex). Our Cu abundances in 3D and with HM are not too different from the results of Shi et al. ([2014](#); 4.19 ± 0.10, from ten lines), Kock & Richter ([1968](#); 4.16 ± 0.08, from six lines) and Sneden & Crocker ([1988](#); 4.12, from two lines). We do not reproduce the rather large difference in abundance found by Shi et al. ([2014](#)) between the low and high excitation lines with the HM model. However, our sample only includes one of the low excitation lines used by those authors. Our adopted value agrees reasonably well with the meteoritic abundance ($\log \epsilon_{\mathrm{Cu}} = 4.25 \pm 0.04$; Lodders et al. [2009](#)).

5.2. Zinc

Our 3D+NLTE zinc abundance is

$$\log \epsilon_{\mathrm{Zn}} = 4.56 \pm 0.05 \ (\pm 0.03 \text{ stat}, \ \pm 0.04 \text{ sys}).$$

We note that the abundance only varies by 0.026 dex when we go from $S_H = 0.1$ to 1. The mean NLTE correction is also
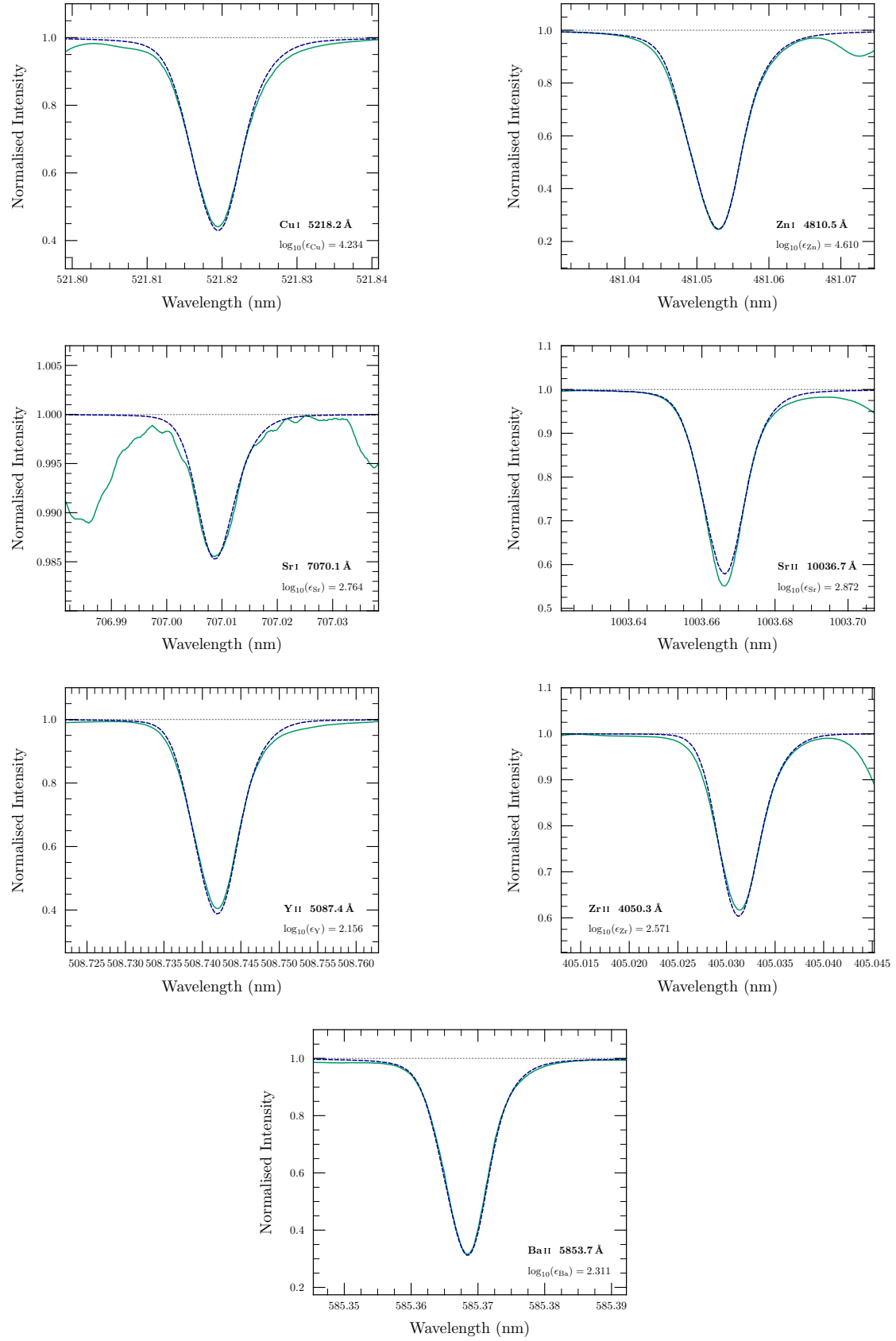
Fig. 1. Example spatially and temporally averaged, disc-centre synthesised line profiles (blue dashed), shown in comparison to the observed FTS profile (solid green). The solar gravitational redshift was removed from the FTS spectrum. The synthesised profiles have been convolved with an instrumental sinc function and fitted in abundance; wavelength and intensity normalisations have been adjusted for display purposes. Note that the plotted profiles are the 3D LTE ones, whereas the quoted abundance in each panel accounts also for the predicted 1D NLTE correction (if available).
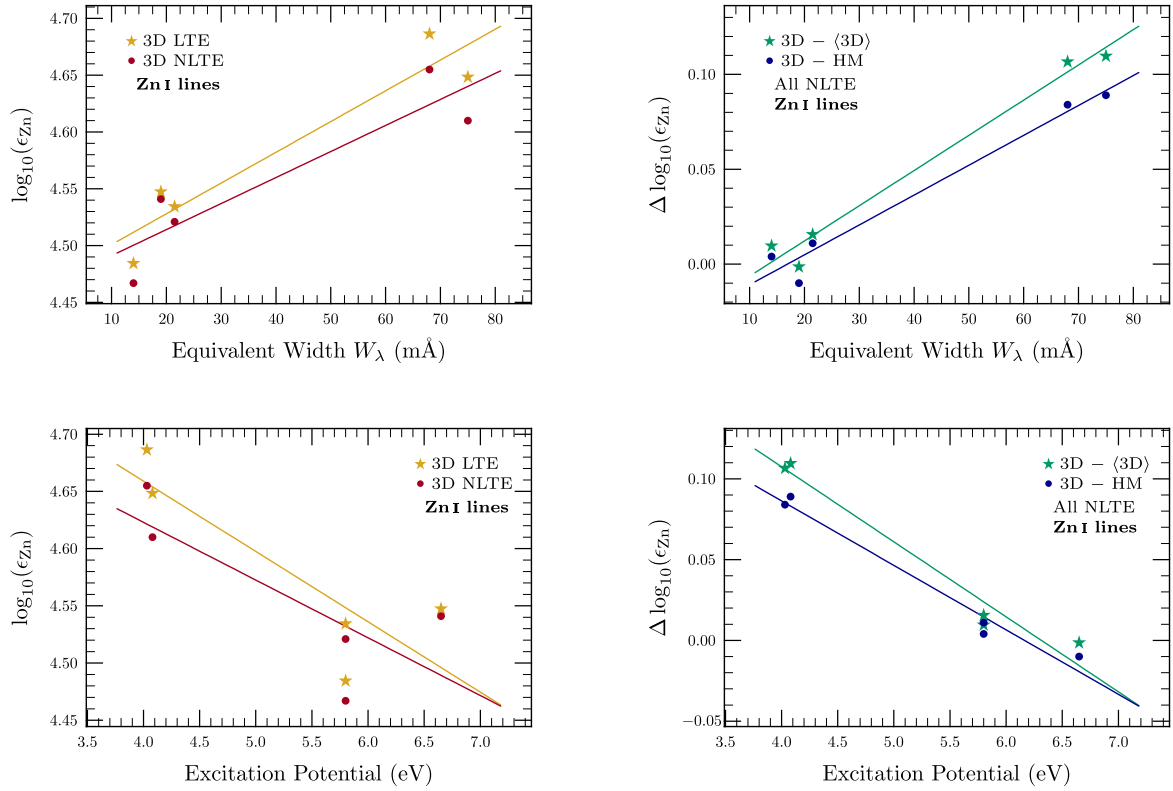
Fig. 2. *Left*: Zn abundances derived from Zn I lines with the 3D model, shown as a function of equivalent width and lower excitation potential. *Right*: line-by-line differences between Zn abundances obtained with the 3D and ⟨3D⟩ models, and between those obtained with the 3D and HM models. Trendlines give equal weight to each line (unlike our mean abundances, where we give larger weights to better lines).

very small: -0.02 dex. Zn I is one of the few species where the HM model gives a slightly lower abundance than the 3D model: $\log \epsilon_{Zn} = 4.53$. Referring to Fig. 2, we see that this is essentially due to two strong lines only, indicating that the microturbulence adopted in 1D is probably too high, or possibly that Doppler broadening due to convection is insufficient in the 3D case. Curiously, these two lines return an abundance approximately 0.1 dex larger with the 3D model than any 1D model, including ⟨3D⟩. This leads to pronounced trends with line strength and excitation potential, although the significance of the trends is debatable given the small number of lines. These are precisely the two lines for which we renormalised oscillator strengths to the scale of Kerkhoff et al. (1980), but this operation amounts to a change of just 0.01 dex, so cannot explain the 0.1 dex offset. Another possibility is that the NLTE corrections may have been underestimated for these high-forming lines, given that they were computed using a 1D model atmosphere, but it seems difficult to believe that this could be a 0.1 dex effect.

Our results are in good agreement with the LTE result of Biémont & Godefroid (1980b; $\log \epsilon_{Zn} = 4.56$ with the HM model), and with Sneden & Crocker's result (1988; $\log \epsilon_{Zn} = 4.62$, based on two lines only). Our final abundance also overlaps the meteoritic one ($\log \epsilon_{Zn} = 4.63 \pm 0.04$; Lodders et al. 2009).

5.3. Gallium

For Ga we find

$$\log \epsilon_{Ga} = 3.02 \pm 0.05 \text{ (pure systematic error)}$$

from the sole Ga I 417.2 nm line. This value is about 0.2 dex higher than the earlier estimates by Ross & Aller (1970) and Lambert et al. (1969), but agrees with the meteoritic abundance ($\log \epsilon_{Ga} = 3.08 \pm 0.02$; Lodders et al. 2009) to within the mutual uncertainties.

5.4. Germanium

For Ge we derive

$$\log \epsilon_{Ge} = 3.63 \pm 0.07 \text{ (pure systematic error)},$$

in reasonable agreement with Biémont et al. (1999) and the meteoritic abundance ($\log \epsilon_{Ge} = 3.58 \pm 0.04$; Lodders et al. 2009).

5.5. Arsenic

We rechecked the two lines at 299.1 and 303.2 nm used previously by Gopka et al. (2001) and could not derive any meaningful abundance, because of the very heavy blending. For this reason, and the unreliable nature of the gf-values for these lines, we conclude that the As abundance cannot be reliably derived from the solar photospheric spectrum.

5.6. Rubidium

With our chosen data, we find

$$\log \epsilon_{Rb} = 2.47 \pm 0.07 \text{ (± 0.06 stat, ± 0.05 sys)}.$$

This value is 0.10 dex lower than the abundance obtained with the HM model. We note however that the 780.0 nm line leads to
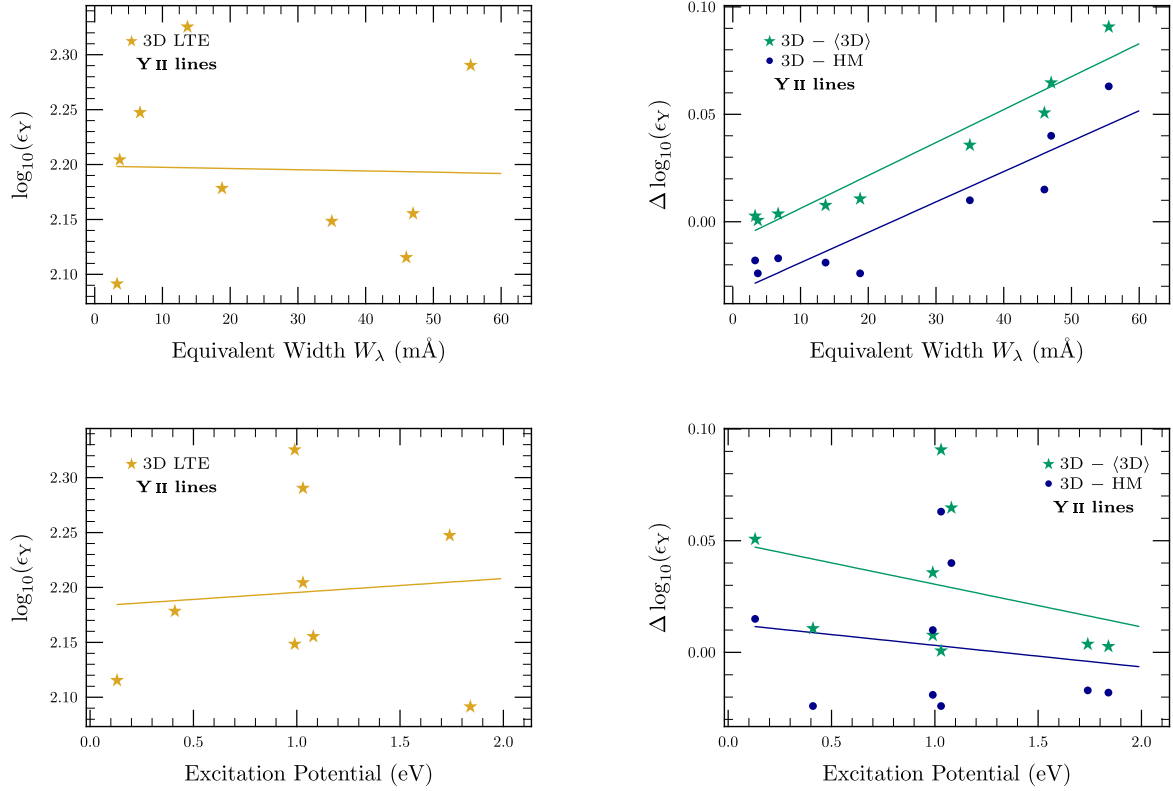
Fig. 3. *Left*: Y abundances from Y II lines in our 3D LTE analysis, as a function of equivalent width and lower excitation potential. *Right*: line-by-line differences between abundances obtained with the 3D and ⟨3D⟩ models, and between those obtained with the 3D and HM models.

an abundance 0.11 dex larger than the 794.7 nm line, suggesting that an unknown blend might contribute about 25% of its equivalent width.

Lambert & Mallia (1968) and Hauge (1972a) analysed these same two lines. Hauge found $\log \epsilon_{Rb}$ = 2.60, in pretty good agreement with Lambert & Mallia's $\log \epsilon_{Rb}$ = 2.63. Our derived Rb abundance is quite a bit lower than both of these values but still significantly above the CI meteoritic value ($\log \epsilon_{Rb}$ = 2.36 ± 0.03; Lodders et al. 2009).

5.7. Strontium

Gratton & Sneden (1994) concluded that the Sr I lines lead to an abundance of $\log \epsilon_{Sr}$ = 2.75, much smaller than the Sr II lines ($\log \epsilon_{Sr}$ = 2.97). However, Barklem & O'Mara (2000) found good agreement between Sr I and Sr II with the same HM atmospheric model, using their new damping parameters. Their final abundance was $\log \epsilon_{Sr}$ = 2.92 ± 0.05.

Our 3D+NLTE results are $\log \epsilon_{Sr}$ = 2.80 ± 0.06 (1σ scatter, Sr I) and $\log \epsilon_{Sr}$ = 2.85 ± 0.08 (1σ scatter, Sr II). Abundances from the two ionisation stages now agree very well in NLTE, whereas in LTE they differ by a factor of two: 2.69 (Sr I) versus 3.02 (Sr II). The mean 3D+NLTE Sr abundance, from all Sr I and Sr II lines together, becomes

$\log \epsilon_{Sr}$ = 2.83 ± 0.06 (±0.02 stat, ±0.05 sys).

This result is substantially lower (by 0.09 dex) than obtained by Barklem & O'Mara, which is also true for our HM-based value. Our recommended value still overlaps the meteoritic Sr abundance ($\log \epsilon_{Zn}$ = 2.88 ± 0.03; Lodders et al. 2009).

5.8. Yttrium

The new 3D LTE abundance is

$\log \epsilon_Y$ = 2.21 ± 0.05 (±0.03 stat, ±0.04 sys).

As seen in Fig. 3, the 3D effect is quite small except for stronger lines, which is as expected for a dominant species like Y II. No appreciable trend can be seen in the 3D results, either in equivalent width or excitation potential. Our result agrees with both that of Hannaford et al. (1982, $\log \epsilon_Y$ = 2.24 ± 0.03) and the meteoritic abundance ($\log \epsilon_Y$ = 2.17 ± 0.04; Lodders et al. 2009).

5.9. Zirconium

The 3D LTE result from our Zr II lines is

$\log \epsilon_{Zr}$ = 2.59 ± 0.04 (±0.01 stat, ±0.04 sys).

We see from Fig. 4 and Table 1 that abundances from Zr II lines, as expected for relatively high excitation lines of a dominant ionisation stage, are quite independent of the adopted photospheric model. The use of the HM model for example leads to exactly the same value of the mean abundance. From Table 1, we also see a very large scatter and strong model-dependence in the Zr I results, as expected for a minor contributor. If we postulate that the four very weak Zr I lines that lead to the smallest abundance are the only Zr I lines that are not blended, these lines return a 3D abundance of $\log \epsilon_{Zr}$ = 2.32 ± 0.07 (1σ), 0.27 dex smaller than the value derived from the Zr II lines. This difference may be explained by the very large NLTE effects on Zr I lines (Velichko et al. 2010, 2011).

Our new result is in perfect agreement with the Zr abundance found by Ljung et al. (2006), from a smaller sample of seven
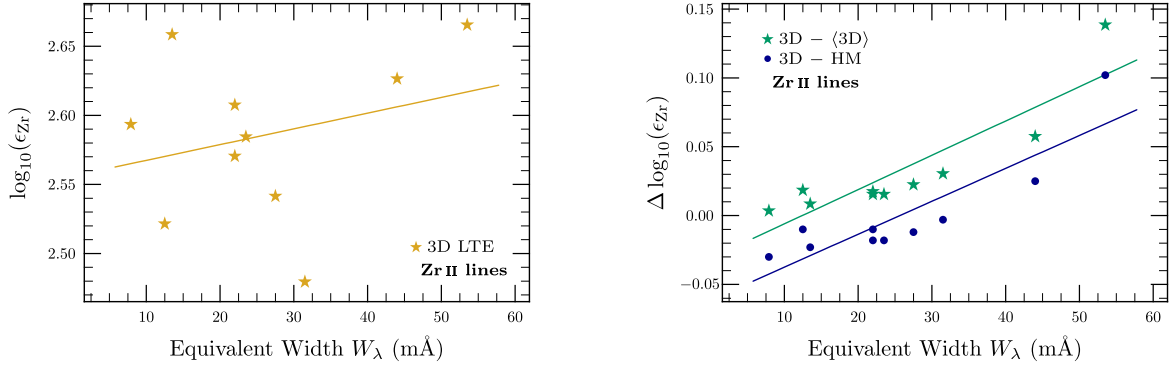
Fig. 4. *Left*: Zr abundances from Zr II lines for the 3D LTE case, as a function of equivalent width. *Right*: line-by-line differences between abundances obtained with the 3D and ⟨3D⟩ models, and between those obtained with the 3D and HM models.
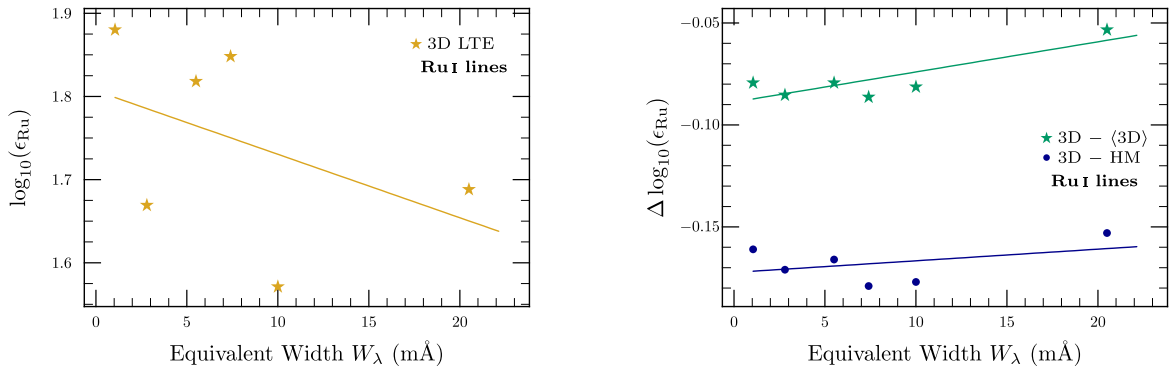

Fig. 5. *Left*: Ru abundances in 3D LTE from Ru I lines, as a function of equivalent width. *Right*: line-by-line differences between abundances obtained with the 3D and ⟨3D⟩ models, and between those obtained with the 3D and HM models.

Zr II lines with wavelengths >400 nm analysed in LTE with an older version of our 3D model. It also overlaps the meteoritic value (log ϵ_{Zr} = 2.53 ± 0.04; Lodders et al. 2009) to within the mutual uncertainties. Caffau et al. (2011a) recently redetermined the solar abundance of Zr using their 3D model. Their 3D LTE result, log ϵ_{Zr} = 2.62 ± 0.06, from a sample of 15 Zr II lines, is slightly larger than ours. This can be explained by their use of the gf-values from Ljung et al. (2006) rather than the mean values we employ, by the different 3D models and by their use of a somewhat larger sample of Zr II lines, including a number of doubtful lines that we suspect might be blended.

5.10. Niobium

We give the raw line-by line results of Nilsson et al. (2010) in the HM column of Table 1, then give in the 3D column the implied 3D abundance for each line, when the 3D-HM correction we have derived here is applied. The final Nb abundance is

log ϵ_{Nb} = 1.47 ± 0.06,

where we have retained the stated error of Nilsson et al. (2010), as it is clear that systematics in the spectral synthesis fitting dominate the error budget in this case. In their paper Nilsson et al. (2010) give log ϵ_{Nb} = 1.47 as the mean of their HM results, but from the results in their Table 8 for the four lines they recommend to use, the mean should be log ϵ_{Nb} = 1.49. They gave a final recommended abundance of log ϵ_{Nb} = 1.44 ± 0.06 after applying a −0.03 dex correction for 3D effects, based on the typical difference 3D-HM we reported for rare earth elements in AGSS09. The mean difference 3D-HM we see here for Nb II

is indeed −0.026 dex. The final abundance agrees with earlier HM-based one of Hannaford et al. (1985; log ϵ_{Nb} = 1.42 ± 0.06), and with the meteoritic abundance (log ϵ_{Nb} = 1.41 ± 0.04; Lodders et al. 2009).

5.11. Molybdenum

We obtain a 3D abundance

log ϵ_{Mo} = 1.88 ± 0.09 (±0.06 stat, ±0.06 sys),

in agreement with Biémont et al. (1983) and the meteoritic abundance (log ϵ_{Mo} = 1.94 ± 0.04; Lodders et al. 2009). The 3D effect is very large for these low-excitation lines of a minority neutral species: −0.16 dex, giving an abundance of log ϵ_{Mo} = 2.04 with the HM model.

5.12. Ruthenium

Using our new 3D model and the experimental gf-values of Wickliffe et al. (1994), the solar Ru abundance becomes

log ϵ_{Ru} = 1.75 ± 0.08 (±0.05 stat, ±0.07 sys).

This is our recommended value, in good agreement with the result of Fivet et al. (2009) and the meteoritic value (log ϵ_{Ru} = 1.76 ± 0.03; Lodders et al. 2009). As can be seen in Fig. 5, 3D effects on Ru I line formation are quite large: approximately −0.08 each from the mean temperature structure and the presence of inhomogeneities, for a total effect of −0.17 dex. No significant trends with equivalent width or excitation potential are evident.

5.13. Rhodium

From our two selected Rh I lines, we get

$$\log \epsilon_{\mathrm{Rh}} = 0.89 \pm 0.08 \ (\pm 0.04 \ \mathrm{stat}, \ \pm 0.07 \ \mathrm{sys}),$$

well below both the result of Kwiatkowski et al. (1982) and the meteoritic abundance (log ϵ_{Ru} = 1.06 ± 0.04; Lodders et al. 2009). The 3D effect is very large (−0.17 dex on average), not surprisingly for a minority neutral species. The photospheric value we recommend is 0.02 dex smaller than in AGSS09.

5.14. Palladium

Our 3D LTE result for Pd is

$$\log \epsilon_{\mathrm{Pd}} = 1.55 \pm 0.06 \ (\pm 0.02 \ \mathrm{stat}, \ \pm 0.06 \ \mathrm{sys}).$$

The 3D effect, −0.06 dex, is smaller than for the other minority species Rb, Zr, Mo, Ru, and Rh, as the ratio ion/neutral is smaller for Pd. The Pd abundance derived with the HM model is log ϵ_{Pd} = 1.61, somewhat lower than found by Xu et al. (2006; log ϵ_{Pd} = 1.66 ± 0.04), due in part to our more stringent line selection. Interestingly, our 3D abundance is substantially lower than the meteoritic one (log ϵ_{Pd} = 1.65 ± 0.02; Lodders et al. 2009).

5.15. Silver

Our 3D LTE solar abundance of silver is

$$\log \epsilon_{\mathrm{Ag}} = 0.96 \pm 0.10 \ (\pm 0.09 \ \mathrm{stat}, \ \pm 0.06 \ \mathrm{sys}),$$

in agreement with the earlier value from Grevesse (1984; log ϵ_{Ag} = 0.94 ± 0.25), but well below the meteoritic abundance (log ϵ_{Ag} = 1.20 ± 0.02; Lodders et al. 2009). The HM-based abundance is significantly larger (1.04), but the presence of atmospheric inhomogeneities, as opposed to the mean stratification, matters little.

5.16. Cadmium

Taking into account the large uncertainty on the measured equivalent width (W_λ = 0.073 ± 0.021 pm) of the one Cd I line available, our 3D solar Cd abundance is

$$\log \epsilon_{\mathrm{Cd}} = 1.77 \pm 0.15 \ (\text{pure systematic error}).$$

The 3D effect is small: −0.03 dex. Our result is coincidentally in perfect agreement with that of Youssef et al. (1990; log ϵ_{Cd} = 1.77 ± 0.11), and also easily overlaps the meteoritic abundance (log ϵ_{Cd} = 1.71 ± 0.03; Lodders et al. 2009).

5.17. Indium

We adopt the solar abundance of In suggested by Vitas et al. (2008):

$$\log \epsilon_{\mathrm{In}} = 0.80 \pm 0.20.$$

Using the meteoritic abundance, the equivalent width of the In I contribution to the observed photospheric feature at 451.13 nm should be 0.055 pm, i.e. In I contributes <20% of the observed faint photospheric line, which has W_λ = 0.33 pm. In principle, the problems in the photosphere might be related to potentially large NLTE and/or 3D effects on In I line formation. If we assume (purely for the sake of argument) that the entire line is In I, then we confirm the high abundance value with the HM model: log ϵ_{In} = 1.61. With the 3D model, we would instead find log ϵ_{In} = 1.46, meaning that 3D effects are indeed large (−0.14 dex after rounding), but certainly not large enough to reconcile the abundance with the meteoritic value. Combining NLTE and 3D effects could never successfully explain the 0.8 dex difference between the photospheric and meteoritic abundances, confirming the conclusion of Vitas et al. (2008) that the photospheric line is severely blended.

5.18. Tin

Taking into account the error on the equivalent width of the single Sn I line we use (in addition to our standard error budget), the 3D result is

$$\log \epsilon_{\mathrm{Sn}} = 2.02 \pm 0.10 \ (\text{pure systematic error}).$$

With the HM model we obtained log ϵ_{Sn} = 2.13, so the 3D effect is rather large: −0.11 dex. A very old solar abundance by Grevesse et al. (1968; log ϵ_{Sn} = 1.32) was revised by Lambert et al. (1969) with a new, more accurate gf-value, and then by Ross & Aller (1976), resulting in log ϵ_{Sn} = 2.0 ± 0.4. Our result is very close to that of Ross & Aller (1976), and is entirely consistent with the meteoritic abundance (log ϵ_{Sn} = 2.07 ± 0.06; Lodders et al. 2009).

5.19. Antimony

Taking into account the large uncertainties of the equivalent width and the experimental gf-values, we find a solar Sb abundance of log $\epsilon_{\mathrm{Sb}} \approx 1.5 \pm 0.3$. For this reason, we do not recommend any photospheric abundance of antimony.

5.20. Barium

For the Sun, the few available Ba II lines have been analysed by Holweger & Müller (1974), Rutten (1978), Gratton & Sneden (1994), Mashonkina et al. (1999) and Mashonkina & Gehren (2000), among others. The most recent estimate of the solar abundance is log ϵ_{Ba} = 2.21 (Mashonkina & Gehren 2000).

We find a 3D+NLTE Ba abundance of

$$\log \epsilon_{\mathrm{Ba}} = 2.25 \pm 0.07 \ (\pm 0.03 \ \mathrm{stat}, \ \pm 0.07 \ \mathrm{sys}).$$

Our HM-based value is actually 0.07 dex lower. Both the HM and 3D results overlap the recommended value of Mashonkina & Gehren (2000), as well as the meteoritic value (log ϵ_{Ba} = 2.18 ± 0.03; Lodders et al. 2009).

5.21. Rare Earths (La to Lu) and Hafnium

As we explain in Sect. 4.21, we do not attempt a detailed 3D-based analysis of all the often-blended lines of rare Earth elements and Hf. Instead we rely on the careful work done by Lawler, Sneden and collaborators using 1D spectrum synthesis with the HM model, and simply correct their derived abundance with our predicted 3D-HM corrections for a subsample of lines (for each element, the lines behave very similarly in this respect so there is no need to compute the 3D effect for all lines). As expected for low excitation lines of a dominant species, the 3D-HM effect on all the rare Earth lines we investigated is small, varying from −0.01 to −0.04 dex. The 3D results for all elements La-Hf are summarised in Table 4.

Table 4. Average abundances implied by all lines of elements from Cu to Th.

	Species	3D	⟨3D⟩	HM	MARCS	MISS	3D-HM	3D-⟨3D⟩	Recommended	Meteoritic
log ε$_{Cu}$	Cu I	4.18 ± 0.05	4.16	4.21	4.11	4.18	−0.03	0.02	4.18 ± 0.05	4.25 ± 0.04
log ε$_{Zn}$	Zn I	4.56 ± 0.05	4.52	4.53	4.46	4.54	0.03	0.04	4.56 ± 0.05	4.63 ± 0.04
log ε$_{Ga}$	Ga I	3.02 ± 0.05	3.00	3.09	2.96	3.02	−0.06	0.02	3.02 ± 0.05	3.08 ± 0.02
log ε$_{Ge}$	Ge I	3.63 ± 0.07	3.55	3.62	3.51	3.57	0.01	0.09	3.63 ± 0.07	3.58 ± 0.04
log ε$_{Kr}$				Interpolated *s*-process production rate (AGSS09)					3.25 ± 0.06	−2.27
log ε$_{Rb}$	Rb I	2.47 ± 0.07	2.52	2.57	2.48	2.54	−0.10	−0.04	2.47 ± 0.07	2.36 ± 0.03
log ε$_{Sr}$	Sr I	2.80 ± 0.06	2.82	2.84	2.77	2.79	−0.03	−0.01		
	Sr II	2.85 ± 0.11	2.75	2.86	2.70	2.86	−0.01	0.09		
	Sr all	2.83 ± 0.06	2.78	2.85	2.73	2.83	−0.02	0.05	2.83 ± 0.06	2.88 ± 0.03
log ε$_{Y}$	Y II	2.21 ± 0.05	2.17	2.20	2.14	2.20	0.01	0.04	2.21 ± 0.05	2.17 ± 0.04
log ε$_{Zr}$	(Zr I)	2.57 ± 0.12	2.67	2.75	2.64	2.69	−0.18	−0.10		
	Zr II	2.59 ± 0.04	2.55	2.59	2.53	2.59	−0.00	0.03	2.59 ± 0.04	2.53 ± 0.04
log ε$_{Nb}$	Nb II	1.47 ± 0.06		1.49			−0.03	0.00	1.47 ± 0.06	1.41 ± 0.04
log ε$_{Mo}$	Mo I	1.88 ± 0.09	1.96	2.04	1.93	1.98	−0.16	−0.08	1.88 ± 0.09	1.94 ± 0.04
log ε$_{Ru}$	Ru I	1.75 ± 0.08	1.82	1.91	1.80	1.84	−0.17	−0.08	1.75 ± 0.08	1.76 ± 0.03
log ε$_{Rh}$	Rh I	0.89 ± 0.08	0.98	1.07	0.95	0.99	−0.17	−0.08	0.89 ± 0.08	1.06 ± 0.04
log ε$_{Pd}$	Pd I	1.55 ± 0.06	1.52	1.61	1.49	1.54	−0.06	0.03	1.55 ± 0.06	1.65 ± 0.02
log ε$_{Ag}$	Ag I	0.96 ± 0.10	0.95	1.04	0.92	0.96	−0.08	0.01	0.96 ± 0.10	1.20 ± 0.02
log ε$_{Cd}$	Cd I	1.77 ± 0.15	1.76	1.79	1.73	1.79	−0.03	0.01	1.77 ± 0.15	1.71 ± 0.03
log ε$_{In}$	In I			Sunspot (Vitas et al. 2008)					0.80 ± 0.20	0.76 ± 0.03
log ε$_{Sn}$	Sn I	2.02 ± 0.10	2.06	2.13	2.04	2.09	−0.11	−0.05	2.02 ± 0.10	2.07 ± 0.06
log ε$_{Xe}$				Interpolated *s*-process production rate (AGSS09)					2.24 ± 0.06	−1.95
log ε$_{Ba}$	Ba II	2.25 ± 0.07	2.15	2.18	2.10	2.17	0.07	0.10	2.25 ± 0.07	2.18 ± 0.03
log ε$_{La}$	La II	1.11 ± 0.04		1.14			−0.03	0.00	1.11 ± 0.04	1.17 ± 0.02
log ε$_{Ce}$	Ce II	1.58 ± 0.04		1.61			−0.03	0.01	1.58 ± 0.04	1.58 ± 0.02
log ε$_{Pr}$	Pr II	0.72 ± 0.04		0.76			−0.04	−0.01	0.72 ± 0.04	0.76 ± 0.03
log ε$_{Nd}$	Nd II	1.42 ± 0.04		1.45			−0.03	0.00	1.42 ± 0.04	1.45 ± 0.02
log ε$_{Sm}$	Sm II	0.95 ± 0.04		0.99			−0.04	−0.01	0.95 ± 0.04	0.94 ± 0.02
log ε$_{Eu}$	Eu II	0.52 ± 0.04		0.55			−0.03	0.00	0.52 ± 0.04	0.51 ± 0.02
log ε$_{Gd}$	Gd II	1.08 ± 0.04		1.11			−0.03	0.01	1.08 ± 0.04	1.05 ± 0.02
log ε$_{Tb}$	Tb II	0.31 ± 0.10		0.28			−0.04	−0.00	0.31 ± 0.10	0.32 ± 0.03
log ε$_{Dy}$	Dy II	1.10 ± 0.04		1.13			−0.03	0.00	1.10 ± 0.04	1.13 ± 0.02
log ε$_{Ho}$	Ho II	0.48 ± 0.11		0.51			−0.03	0.00	0.48 ± 0.11	0.47 ± 0.03
log ε$_{Er}$	Er II	0.93 ± 0.05		0.96			−0.03	0.01	0.93 ± 0.05	0.92 ± 0.02
log ε$_{Tm}$	Tm II	0.11 ± 0.04		0.14			−0.03	0.01	0.11 ± 0.04	0.12 ± 0.03
log ε$_{Yb}$	Yb II	0.85 ± 0.11		0.86			−0.01	0.03	0.85 ± 0.11	0.92 ± 0.02
log ε$_{Lu}$	Lu II	0.10 ± 0.09		0.12			−0.02	0.00	0.10 ± 0.09	0.09 ± 0.02
log ε$_{Hf}$	Hf II	0.85 ± 0.05		0.88			−0.03	0.00	0.85 ± 0.05	0.71 ± 0.02
log ε$_{W}$	W I	0.83 ± 0.11		1.03			−0.19	−0.09	0.83 ± 0.11	0.65 ± 0.04
log ε$_{Os}$	Os I	1.40 ± 0.05	1.41	1.50	1.40	1.44	−0.09	−0.01	1.40 ± 0.05	1.35 ± 0.03
log ε$_{Ir}$	Ir I	1.42 ± 0.07	1.40	1.46	1.38	1.43	−0.04	0.02	1.42 ± 0.07	1.32 ± 0.02
log ε$_{Au}$	Au I	0.91 ± 0.08	0.89	0.93	0.88	0.93	−0.02	0.02	0.91 ± 0.08	0.80 ± 0.04
log ε$_{Tl}$	Tl I			Sunspot (Lambert et al. 1972)					0.9 ± 0.2	0.77 ± 0.03
log ε$_{Pb}$	Pb I	1.92 ± 0.08	1.97	2.05	1.95	2.00	−0.14	−0.06	1.92 ± 0.08	2.04 ± 0.03
log ε$_{Th}$	Th II	0.03 ± 0.10	0.03	0.07	0.02	0.06	−0.04	−0.00	0.03 ± 0.10	0.06 ± 0.03

Notes. Abundances are given as the weighted mean across all lines in the given list, taking into account NLTE corrections for Zn I, Sr I, Sr II, Ba II, Eu II, Pb I and Th II. Zr I is shown in brackets because we do not consider this result reliable enough to include in our final adopted abundance. Note that because all means were computed using abundances accurate to three decimal places, entries in Cols. 8 and 9 differ in some cases from the differences between the entries in Cols. 3−5. We also give our final recommended solar photospheric abundance of each element, compared with the abundance in CI chondritic meteorites (Lodders et al. 2009, normalised to the silicon abundance determined in Paper I).

Updating the original Sm abundance of Lawler et al. for the new gf-values we describe in Sect. 4.21 leads to a small change in the HM abundance: $\log \epsilon_{Sm} = 0.99$ instead of 1.00.

Our 3D LTE result for Eu, $\log \epsilon_{Eu} = 0.49$, is 0.03 dex lower than the recent LTE Eu solar abundance found by Mucciarelli et al. (2008; $\log \epsilon_{Eu} = 0.52$), using their own 3D model. Our recommended Eu abundance however also includes NLTE corrections of +0.03 dex from Mashonkina & Gehren (2000), which cancel the 3D correction of −0.03 dex to bring our final result into (coincidentally) perfect agreement with those of both Mucciarelli et al. (2008) and Lawler et al. (2001b).

With the 3D model, the one Tb II line we retained returns $\log \epsilon_{Tb} = 0.31 \pm 0.10$. If we had kept all three lines analysed by Lawler et al. (2001c), we would have obtained an abundance of $\log \epsilon_{Tb} = 0.24 \pm 0.08$.

Our new Hf abundance, $\log \epsilon_{Hf} = 0.85 \pm 0.05$, is in very good agreement with a recent result by Caffau et al. (2008) using their own 3D model: $\log \epsilon_{Hf} = 0.87 \pm 0.04$. Although the solar abundances of all elements from La to Lu are consistent with the meteoritic values (to within the mutual uncertainties), the solar abundance of Hf is quite a bit higher than the meteoritic one ($\log \epsilon_{Hf} = 0.71 \pm 0.02$; Lodders et al. 2009). Perhaps the most natural explanation would be erroneous gf-values for the Hf II lines, but the experimental data from Lawler et al. (2007) appear reliable.

5.22. Tungsten

Updating the results of Holweger & Werner (1982) for the new gf-values we discuss in Sect. 4.22, the mean abundance becomes $\log \epsilon_W = 1.03$. We further updated this result by computing the 3D-HM abundance corrections for these two lines: −0.19 dex. This is not surprising for these low excitation lines of a minor species (W II/W I ∼ 10). The 3D LTE abundance of W thus becomes

$\log \epsilon_W = 0.83 \pm 0.11$ (±0.03 stat, ±0.11 sys),

where the systematic error includes both the regular sources (0.08 dex) and the error in the equivalent widths (0.07 dex), due to the fact that these lines are very weak (0.35 and 0.035 pm respectively, cf. Table 1). Even with spectral synthesis these lines are extremely difficult to reproduce accurately. Despite the large 3D effects, the solar tungsten abundance is substantially larger than seen in meteorites ($\log \epsilon_W = 0.65 \pm 0.04$; Lodders et al. 2009), similar to the case of Hf mentioned above.

5.23. Osmium

We find with our 3D model an Os abundance of

$\log \epsilon_{Os} = 1.40 \pm 0.05$ (pure systematic error),

in reasonable agreement with the meteoritic value ($\log \epsilon_{Os} = 1.35 \pm 0.03$; Lodders et al. 2009). The 3D effect is quite large: −0.09 dex.

An example of the problem with the Os I lines used in past analyses is seen in the results of Kwiatkowsky et al. (1984): the dispersion is very large ($\sigma = 0.15$ dex), and the difference between the lowest and largest abundances is 0.42 dex. Recent results by Caffau et al. (2011b), who used the lines and solar data of Kwiatkowsky et al. with their own 3D model, show a similarly unacceptable dispersion. Their result, $\log \epsilon_{Os} = 1.36 \pm 0.19$ dex, includes a striking difference of 0.71 dex between the lowest

and largest abundance. We note that Caffau et al. used an obsolete value for the ionisation potential of Os I (8.7 eV), whereas the correct value is 8.4382 ± 0.0002 eV (Colarusso et al. 1997). We estimate that their abundance results from Os I lines should therefore be increased by about 0.15 dex, to $\log \epsilon_{Os} = 1.51 \pm 0.19$ dex. This result is much larger than what we find here, as expected from the severely blended nature of some of their chosen lines.

5.24. Iridium

With our adopted equivalent width and gf-value, we find a 3D abundance of

$\log \epsilon_{Ir} = 1.42 \pm 0.07$ (pure systematic error),

where the error includes the uncertainty in the measured equivalent width (0.06 dex) and the combined contributions of the usual three systematics (0.04 dex). This abundance is in rather poor agreement with the meteoritic value ($\log \epsilon_{Ir} = 1.32 \pm 0.02$; Lodders et al. 2009). Our result is however consistent with previous determinations: Youssef & Khalil (1988) found $\log \epsilon_{Ir} = 1.38 \pm 0.05$, and the result of Drake & Aller (1976) goes from $\log \epsilon_{Ir} = 0.82$ to $\log \epsilon_{Ir} = 1.37$ when updated to the gf-value we adopt.

5.25. Gold

We find a 3D solar gold abundance of

$\log \epsilon_{Au} = 0.91 \pm 0.08$ (pure systematic error),

where we have incorporated the uncertainty in the equivalent width and gf-value into the final uncertainty. The 3D effect is small: −0.02 dex. Updating the HM spectrum synthesis result of Youssef (1986; $\log \epsilon_{Au} = 0.95$) with the 3D-HM effect would lead to $\log \epsilon_{Au} = 0.93$, in excellent agreement with the value we obtain here. Our adopted gold abundance remains substantially higher than the meteoritic value ($\log \epsilon_{Au} = 0.80 \pm 0.04$; Lodders et al. 2009).

5.26. Lead

The LTE abundances of lead with the 3D and HM models are $\log \epsilon_{Pb} = 1.80$ and 1.93, respectively; the 3D-HM effect is rather large, −0.14 dex after rounding. This is expected because Pb I is a minority species compared to Pb II in the solar photosphere.

Taking into account the significant NLTE correction (+0.12 dex) of Mashonkina et al. (2012), our final 3D abundance of Pb becomes

$\log \epsilon_{Pb} = 1.92 \pm 0.08$ (pure systematic error).

This is somewhat smaller than obtained by Biémont et al. (2000; $\log \epsilon_{Pb} = 2.00 \pm 0.06$) with the HM model and an erroneously large equivalent width. Our photospheric Pb abundance is also substantially smaller than the corresponding CI meteoritic value ($\log \epsilon_{Pb} = 2.04 \pm 0.03$; Lodders et al. 2009).

5.27. Thorium

The 3D+NLTE solar abundance of Th is

$\log \epsilon_{Th} = 0.03 \pm 0.10$ (pure systematic error),

where the error budget is dominated by the uncertainty in our adopted equivalent width. Given the overall uncertainty, the photospheric abundance of Th is consistent with the meteoritic value ($\log \epsilon_{Th} = 0.06 \pm 0.03$; Lodders et al. 2009). With the HM model, the abundance would be $\log \epsilon_{Th} = 0.07$.

Our 3D LTE abundance is 15% smaller than the corresponding LTE result of Caffau et al. (2008), who found $\log \epsilon_{Th} = 0.08 \pm 0.03$ with their 3D model. The 0.06 dex difference with our LTE result can be explained by our improved, model-independent estimation of the contributions of the blends by Co I and V I. In our opinion the stated uncertainty of Caffau et al. underestimates the uncertainty of the total contribution of Th II to the overall equivalent width.

5.28. Other heavy elements

Many other elements such as Se, Br, Kr, Te, I, Xe, Cs, Ta, Re, Pt, Hg, Tl, Bi, and U are not present in the solar photospheric spectrum. For most of them, the meteoritic abundances have to be adopted as the de facto solar abundances. For Kr and Xe however, solar abundances can be estimated from interpolation of the theoretical s-process production rates. The values for Xe and Kr in Table 4 have been taken from AGSS09. For Tl, a line of Tl I is present in the sunspot spectrum, but heavily blended. This line has been used by Lambert et al. (1972) to derive a very uncertain solar Tl abundance: $\log \epsilon_{Tl} = 0.72$–$1.07$. We shall adopt $\log \epsilon_{Tl} = 0.9 \pm 0.2$.

6. Discussion

In some species of the heavy elements we see large differences between the abundances derived with the 3D model and the four 1D models. The easiest way to understand these differences is to separate the elements into two groups: majority (most of the element is in this ionisation stage, in most cases the once ionised species) and minority (mostly neutral species of elements with relatively low ionisation energy). For majority elements with weak, low-excitation lines, the 3D effect and the differences between the various model atmospheres are small (of order 10% or lower), as these lines form rather deep in the photosphere and are not strongly sensitive to temperature. In this group we find Nb II, Cd I, the rare Earths, Hf II, Ir I, Au I, and Th II. It is clear that the lines of these tracers are not very sensitive to the temperature structure of the model atmosphere: in the rather deep layers where these lines are formed, the mean temperature structures of the different models are quite similar. However, for majority elements with stronger lines such as Zn I, Sr II, Y II, Zr II, and Ba II, we see that the 3D effects and dependence on the model atmosphere often become much larger. These lines are formed significantly higher in the photosphere, where the mean temperature structure of the model atmospheres differ far more.

For the minority elements Cu I, Ga I, Ge I, Rb I, Sr I, Mo I, Ru I, Rh I, Pd I, Ag I, Sn I, W I, Os I, and Pb I, all lines are extremely temperature-sensitive. This is why we observe large differences in abundance results from these lines with different model atmospheres. These differences however depend subtly on the characteristics of each line, and its mean optical depth of formation. We caution that such lines are likely sensitive to departures from LTE, which in most cases have been explored theoretically neither in 1D nor 3D.

Table 5. Recommended present-day solar photospheric abundances for the heavy elements Cu to Th, compared with oft-used solar abundance compilations: AG89 (Anders & Grevesse 1989), GS98 (Grevesse & Sauval 1998), AGS05 (Asplund et al. 2005), AGSS09 (Asplund et al. 2009), LPG09 (Lodders et al. 2009).

Z	el.	Preferred	AG89	GS98	AGS05	AGSS09	LPG09
29	Cu	4.18 ± 0.05	4.21	4.21	4.21	4.19	4.21
30	Zn	4.56 ± 0.05	4.60	4.60	4.60	4.56	4.62
31	Ga	3.02 ± 0.05	2.88	2.88	2.88	3.04	2.88
32	Ge	3.63 ± 0.07	3.41	3.41	3.58	3.65	3.58
36	Kr	3.25 ± 0.06^1			3.28	3.25	3.28
37	Rb	2.47 ± 0.07	2.60	2.60	2.60	2.52	2.60
38	Sr	2.83 ± 0.06	2.90	2.97	2.92	2.87	2.92
39	Y	2.21 ± 0.05	2.24	2.24	2.21	2.21	2.21
40	Zr	2.59 ± 0.04	2.60	2.60	2.59	2.58	2.58
41	Nb	1.47 ± 0.06	1.42	1.42	1.42	1.46	1.42
42	Mo	1.88 ± 0.09	1.92	1.92	1.92	1.88	1.92
44	Ru	1.75 ± 0.08	1.84	1.84	1.84	1.75	1.84
45	Rh	0.89 ± 0.08	1.12	1.12	1.12	0.91	1.12
46	Pd	1.55 ± 0.06	1.69	1.69	1.69	1.57	1.66
47	Ag	0.96 ± 0.10	0.94	0.94	0.94	0.94	0.94
48	Cd	1.77 ± 0.15	1.86	1.77	1.77		1.77
49	In	0.80 ± 0.20^2	1.66	1.66	1.60	0.80	1.50
50	Sn	2.02 ± 0.10	2.00	2.00	2.00	2.04	2.00
54	Xe	2.24 ± 0.06^1			2.27	2.24	2.27
56	Ba	2.25 ± 0.07	2.13	2.13	2.17	2.18	2.17
57	La	1.11 ± 0.04	1.22	1.17	1.13	1.10	1.14
58	Ce	1.58 ± 0.04	1.55	1.58	1.58	1.58	1.61
59	Pr	0.72 ± 0.04	0.71	0.71	0.71	0.72	0.76
60	Nd	1.42 ± 0.04	1.50	1.50	1.45	1.42	1.45
62	Sm	0.95 ± 0.04	1.00	1.01	1.01	0.96	1.00
63	Eu	0.52 ± 0.04	0.51	0.51	0.52	0.52	0.52
64	Gd	1.08 ± 0.04	1.12	1.12	1.12	1.07	1.11
65	Tb	0.31 ± 0.10	−0.10	−0.10	0.28	0.30	0.28
66	Dy	1.10 ± 0.04	1.10	1.14	1.14	1.10	1.13
67	Ho	0.48 ± 0.11	0.26	0.26	0.51	0.48	0.51
68	Er	0.93 ± 0.05	0.93	0.93	0.93	0.92	0.96
69	Tm	0.11 ± 0.04	0.00	0.00	0.00	0.10	0.14
70	Yb	0.85 ± 0.11	1.08	1.08	1.08	0.84	0.86
71	Lu	0.10 ± 0.09	0.76	0.06	0.06	0.10	0.12
72	Hf	0.85 ± 0.05	0.88	0.88	0.88	0.85	0.88
74	W	0.83 ± 0.11	1.11	1.11	1.11	0.85	1.11
76	Os	1.40 ± 0.05	1.45	1.45	1.45	1.40	1.45
77	Ir	1.42 ± 0.07	1.35	1.35	1.38	1.38	1.38
79	Au	0.91 ± 0.08	1.01	1.01	1.01	0.92	1.01
81	Tl	0.90 ± 0.20^3	0.90	0.90	0.90	0.90	0.95
82	Pb	1.92 ± 0.08	1.85	1.95	2.00	1.75	2.00
90	Th	0.03 ± 0.10	0.12			0.02	

Notes. Preferred values are from this work except where noted.

References. [1] AGSS09; [2] Vitas et al. (2008); [3] Lambert et al. (1972).

7. Comparison with previous solar abundance compilations

Table 5 compares our recommended present-day photospheric abundances for the Sun with those advocated by previous, commonly-used compilations of the solar chemical composition. In most cases the differences are relatively minor (± 0.05 dex), although our Ga ($+0.14$ dex compared with Lodders et al. 2009 for example), Rb (-0.13 dex), Sr (-0.09), Ru (-0.09 dex), Rh (-0.23 dex), Pd (-0.09 dex), In (-0.70 dex), Ba ($+0.08$ dex), W (-0.28 dex), Au (-0.10 dex), and Pb (-0.08 dex) abundances show greater variations relative to recent compilations. In many of these cases the previous recommended values were based on

very old analyses, often with outdated atomic data and poor treatment of blends, whereas here we carry out new 3D-based analyses for these elements.

Compared with AGSS09 there have only been minor adjustments (±0.02) of the recommended solar abundances for most elements. Notable exceptions for which larger differences are present are Rb (−0.05 dex), Sr (−0.04 dex), Ba (+0.07 dex), Ir (+0.04 dex) and Pb (+0.17 dex). In most cases, these changes have been driven by improved transition probabilities and/or the appearance of (new) NLTE calculations.

We will comment on the agreement between photospheric and meteoritic abundances in more detail in future work, so we restrict ourselves here to some brief comments. Ignoring the noble gases (in which CI chondritic meteorites are heavily depleted), the photospheric excesses of 0.10 dex or more that we see relative to the CI chondrites for Rb, Hf, W, Ir, and Au might be due to unidentified blends and/or continuum placement. For Rh, Pd, Ag, and Pb, which are under-abundant in the Sun compared to meteorites, one might postulate unidentified or underestimated NLTE effects: the photospheric lines we have used of Rh I, Pd I, Ag I, and Pb I are rather low-excitation lines of minority species, so are expected to be prone to NLTE effects.

8. Conclusions

In this paper we have redetermined the solar abundances of almost every element from Cu to Th, using a new, highly realistic 3D hydrodynamic model of the solar atmosphere. In most cases we have based our determination on a full reanalysis of the relevant lines in the solar spectrum, including the latest atomic data and extremely demanding line selection. We have accounted for departures from LTE wherever such corrections exist. In some cases, where other authors have already performed very detailed and careful analyses based on full spectrum synthesis, we have computed the net impact on the relevant lines of using our 3D model, and adjusted the previous 1D results accordingly. Together with the results of Papers I and II, the results we present here make up the first fully complete, detailed and homogeneous analysis of the medium-and-heavy-element ($Z > 8$) composition of the Sun.

References

Allende Prieto, C., Barklem, P. S., Asplund, M., & Ruiz Cobo, B. 2001, ApJ, 558, 830
Anders, E., & Grevesse, N. 1989, Geochim. Cosmochim. Acta, 53, 197
Asplund, M. 2005, ARA&A, 43, 481
Asplund, M., Gustafsson, B., Kieselman, D., & Eriksson, K. 1997, A&A, 318, 521
Asplund, M., Nordlund, A., Trampedach, R., Allende Prieto, C., & Stein, R. F. 2000, A&A, 359, 729
Asplund, M., Grevesse, N., & Sauval, A. J. 2005, in ASP Conf. Ser. 336, eds. T. G. Barnes III, & F. N. Bash (San Francisco: Astron. Soc. Pac.), 25
Asplund, M., Grevesse, N., Sauval, A. J., & Scott, P. 2009, ARA&A, 47, 481 (AGSS09)
Banerjee, A., Das, D., & Natarajan, V. 2004, Europhys. Lett., 65, 172
Barklem, P. S., & O'Mara, B. J. 2000, MNRAS, 311, 535
Barklem, P. S., Piskunov, N., & O'Mara, B. J. 2000, A&AS, 142, 467
Beacham, J. R., & Andrew, K. L. 1971, JOSA, 61, 231
Beck, D. R. 1992, Phys. Rev. A, 45, 1399
Bielski, A. 1975, J. Quant. Spectr. Rad. Transf., 15, 463
Biémont, E., & Godefroid, M. 1980a, Phys. Scr., 22, 231
Biémont, E., & Godefroid, M. 1980b, A&A, 84, 361
Biémont, E., Grevesse, N., Hannaford, P., & Lowe, R. M. 1981, ApJ, 248, 867
Biémont, E., Grevesse, N., Kwiatkowski, M., & Zimmermann, P. 1982, A&A, 108, 127
Biémont, E., Grevesse, N., Hannaford, P., Lowe, R. M., & Whaling, W. 1983, ApJ, 275, 889
Biémont, E., Lynga, C., Li, Z. S., et al. 1999, MNRAS, 303, 721
Biémont, E., Garnir, H. P., Palmeri, P., Li, Z. S., & Svanberg, S. 2000, MNRAS, 312, 116
Biémont, E., Blagoev, K., Engström, L., et al. 2011, MNRAS, 414, 3350
Bize, S., Sortais, Y., Santos, M. S., et al. 1999, Europhys. Lett., 45, 558
Bord, D. J., & Cowley, C. R. 2001, BAAS, 33, 1433
Bord, D. J., & Cowley, C. R. 2002, Sol. Phys., 211, 3
Brix, P., Kopfermann, H., Martin, R., & Walcher, W. 1951, Z. Phys., 130, 88
Burbidge, E. M., Burbidge, G. R., Fowler, W. A., & Hoyle, F. 1957, Rev. Mod. Phys., 29, 547
Busso, M., Gallino, R., Lambert, D. L., Travaglio, C., & Smith, V. V. 2001, ApJ, 557, 802
Butcher, H. R. 1987, Nature, 328, 127
Caffau, E., Sbordone, L., Ludwig, H.-G., et al. 2008, A&A, 483, 591
Caffau, E., Faraggiana, R., Ludwig, H.-G., Bonifacio, P., & Steffen, M., 2011a, Astron. Nachr., 332, 128
Caffau, E., Ludwig, H.-G., Steffen, M., Freytag, B., & Bonifacio, P. 2011b, Sol. Phys., 268, 255
Cameron, A. G. W. 1957, AJ, 62, 9
Carlsson, J., Sturesson, L., & Svanberg, S. 1989, Z. Phys. D, 11, 287
Carlsson, J., Jönsson, P., & Sturesson, L. 1990, Z. Phys. D, 16, 87
Cayrel, R., Hill, V., Beers, T. C., et al. 2001, Nature, 409, 691
Chan, Y. W., Childs, W. J., & Goodman, L. S. 1968, Phys. Rev., 173, 107
Civiš, S., Matulková, I., Cihelka, et al. 2010, Phys. Rev. A, 82, 022502
Colarusso, P., Lebeault-Dorget, M. A., & Simart, B. 1997, Phys. Rev. A, 55, 1526
Corliss, C. H., & Bozman, W. R. 1962, NBS Monograph, 53
Crawford, M. F., Schawlow, A. L., Gray, W. M., & Kelly, F. M. 1949, Phys. Rev., 75, 1112
Cunningham, P. T., & Link, J. K. 1967, JOSA, 57, 1000
Davidson, M. D., Snoek, L. C, Volten, H., & Dönszelmann, A. 1992, A&A, 255, 457
Delbouille, L., Neven, L., & Roland, G. 1973, Atlas photométrique du spectre solaire de λ3000 a λ10000 (Institut d'Astrophysique, Université de Liège)
Delbouille, L., Roland, G., Brault, J. W., & Testerman, L. 1981, Photometric Atlas of the Solar Spectrum from 1850 to 10 000 cm⁻¹ (Tucson: Kitt Peak National Observatory)
Den Hartog, E. A., Duquette, D. W., & Lawler, J. E. 1987, JOSA, B4, 48
Den Hartog, E. A., Lawler, J. E., Sneden, C., & Cowan, J. J. 2003, ApJS, 148, 543
Den Hartog, E. A., Lawler, J. E., Sneden, C., & Cowan, J. J. 2006, ApJS, 167, 292
Dinneen, T. P., Berrah Mansour, N., Kurtz, C., & Young, L. 1991, Phys. Rev. A, 43, 4824
Drake, S., & Aller, L. H. 1976, Proc. Nat. Acad. Sci. USA, 73, 269
Duquette, D. W., & Lawler, J. E. 1985, JOSAB, 2, 1948
Engleman, R., Litzén, U., Lundberg, H., & Wyart, J.-F. 1998, Phys. Scr, 57, 345
Fischer, W., Hühnermann, H., & Kollath, K.-J. 1967, Z. Phys. 200, 158
Fivet, V., Quinet, P., Palmeri, P., et al. 2009, MNRAS, 396, 2124
Frebel, A., Christlieb, N., Norris, J. E., et al. 2007, ApJ, 660, L117
Gaarde, M. B., Zerne, R., Caiyan, L., et al. 1994, Phys. Rev. A, 50, 209
Gallagher, A. 1967, Phys. Rev., 157, 24
Garcia, G., & Campos, J. 1988, J. Quant. Spectr. Rad. Transf., 39, 477
Golovin, A. F., & Striganov, A. R. 1968, Sov. Phys. Usp., 10, 658
Gonzalez, G. 2006, MNRAS, 371, 781
Gonzalez, A. M., Ortiz, M., & Campos, J. 1997, J. Quant. Spectr. Rad. Transf., 57, 825
Gopka, V. F., Yushchenko, A. V., Shavrina, A. V., Andrievsky, S. M., & Chernysheva, L. V. 2001, KFNT 17, 37
Goriely, S., Bauswein, A., & Janka, H.-T. 2011, ApJ, 738, L32
Gough, D. S., Hannaford, P., & Lowe, R. M. 1983, J. Phys. B, 16, 785

Gratton, R. G., & Sneden, C. 1994, A&A, 287, 927
Grevesse, N. 1984, Phys. Script. T8, 49
Grevesse, N., & Sauval, A. J. 1998, Space Sci. Rev., 85, 161
Grevesse, N., Boury, A., & Blanquet, G. 1968, in Origin and Distribution of the Elements, ed. L. H. Ahrens (New York: Pergamon Press), 177
Guern, Y., & Lotrian, J. 1980, J. Quant. Spectr. Rad. Transf., 24, 133
Gustafsson, B., Edvardsson, B., Eriksson, K., et al. 2008, A&A, 486, 951
Hannaford, P., & McDonald, D. C. 1978, J. Phys. B, 11, 1177
Hannaford, P., & Lowe, R. M. 1983, Opt. Eng., 22, 532
Hannaford, P., Larkins, P. L., & Lowe, R. M. 1981, J. Phys. B, 14, 2321
Hannaford, P., Lowe, R. M., Grevesse, N., Biémont, E., & Whaling, W. 1982, ApJ, 261, 736
Hannaford, P., Lowe, R. M., Biémont, E., & Grevesse, N. 1985, A&A, 143, 447
Hauge, O. 1972a, Sol. Phys., 26, 263
Hauge, O. 1972b, Sol. Phys., 26, 276
Holweger, H., & Müller, E. A. 1974, Sol. Phys., 39, 19
Holweger, H., & Werner, K. 1982, Sol. Phys., 81, 3
Hughes, R. H. 1961, Phys. Rev., 121, 499
Ivarsson, S., Andersen, J., Nordström, B., et al. 2003, A&A, 409, 1141
Jackson, D., & Kuhn, H. 1937, Proc. Roy. Soc. London, Ser. A, 158, 372
Karakas, A. I., García-Hernández, D. A., & Lugaro, M. 2012, ApJ, 751, 8
Kerkhoff, H., Schmidt, M., & Zimmermann, P. 1980, Z. Phys. A, 298, 249
Kling, R., & Kock, M. 1999, J. Quant. Spectr. Rad. Transf., 62, 129
Kobayashi, C., & Nakasato, N. 2011, ApJ, 729, 16
Kock, M., & Richter, J. 1968, Z. Astrophys., 69, 180
Kurucz, R. L. 1998, http://kurucz.harvard.edu/
Kurz, N., Dietrich, M. R., Shu, Gang, et al. 2008, Phys. Rev. A, 77, 060501
Kuske, P., Kirchner, N., Wittmann, W., Andrä, H. J., & Kaiser, D. 1978, Phys. Lett. A, 64, 377
Kwiatkowski, M., Zimmermann, P., Biémont, E., & Grevesse, N. 1982, A&A, 112, 337
Kwiatkowski, M., Zimmermann, P., Biémont, E., & Grevesse, N. 1984, A&A, 135, 59
Lambert, D. L., & Mallia, E. A. 1968, MNRAS, 140, 13
Lambert, D. L., Mallia, E. A., & Warner, B. 1969, MNRAS, 142, 71
Lambert, D. L., Mallia, E. A., & Smith, G. 1972, Sol. Phys., 26, 250
Lawler, J. E., Whaling, W., & Grevesse, N. 1990, Nature, 346, 635
Lawler, J. E., Bonvallet, G., & Sneden, C. 2001a, ApJ, 556, 452
Lawler, J. E., Wickliffe, M. E., Den Hartog, E. A., & Sneden, C. 2001b, ApJ, 563, 1075
Lawler, J. E., Wickliffe, M. E., Cowley, C. R., & Sneden, C. 2001c, ApJS, 137, 341
Lawler, J. E., Sneden, C., & Cowan, J. J. 2004, ApJ, 604, 850
Lawler, J. E., Den Hartog, E. A., Sneden, C., & Cowan, J. J. 2006, ApJS, 162, 227
Lawler, J. E., Den Hartog, E. A., Labby, Z. E., et al. 2007, ApJS, 169, 120
Lawler, J. E., Sneden, C., Cowan, et al. 2008, ApJS, 178, 71
Lawler, J. E., Sneden, C., Cowan, J., Ivans, I., & Den Hartog, E. A. 2009, ApJS, 182, 51
Learner, R. C. M., Davies, J., & Thorne, A. P. 1991, MNRAS, 248, 414
Li, R., Rehse, S. J., Scholl, T. J., et al. 2007, Can. J. Phys., 85, 1343
Ljung, G., Nilsson, H., Asplund, M.,& Johansson, S. 2006, A&A, 456, 1181
Lodders, K., Palme, H., & Gail, H.-P. 2009, Landolt Börnstein, New Series, Vol. VI/4B, Chap. 4.4, Abundances of the Elements in the Solar System, ed. J. E. Trümper (Berlin: Springer-Verlag), 560
Lotrian, J., Cariou, J., & Johannin-Gilles, A. 1976, J. Quant. Spectr. Rad. Transf., 16, 315
Mashonkina, L. I., & Gehren, T. 2000, A&A, 364, 249
Mashonkina, L. I., & Gehren, T. 2001, A&A, 376, 232
Mashonkina, L. I., Gehren, T., & Bikmaiev, I. F. 1999, A&A, 343, 519
Mashonkina, L. I., Ryabtsev, A., & Frebel, A. 2012, A&A, 540, A98
Meggers, W. F., Corliss, C. H., & Scribner, B. F. 1961, Tables of spectral-line intensities (Washington, USA: Monograph 32, National Bureau of Standards, US Dept. of Commerce)
Migdalek, J., & Baylis, W. E. 1987, Can. J. Phys., 65, 1612
Morton, D. C. 2000, ApJS, 130, 403
Mucciarelli, A., Caffau, E., Freytag, B., Ludwig, H.-G., & Bonifacio, P. C. 2008, A&A, 484, 841
Neckel, H., & Labs, D. 1984a, Sol. Phys., 90, 205

Neckel, H., & Labs, D. 1984b, Sol. Phys., 92, 391
Nez, F., Biraben, F., Felder, R., & Millerioux, Y. 1993, Opt. Comm., 102, 432
Nilsson, H., & Ivarsson, S. 2008, A&A, 492, 609
Nilsson, H., Zhang, Z. G., Lundberg, H., Johansson, S., & Nordström, B. 2002, A&A, 382, 368
Nilsson, H., Hartman, H., Engström, L., et al. 2010, A&A, 511, A16
Pereira, T. M. D., Asplund, M., Collet, R., et al. 2013, A&A, 554, A118
Pickering, J. C., & Semeniuk, J. I. 1995, MNRAS, 274, L37
Pignatari, M., Gallino, R., Meynet, G., et al. 2008, ApJ, 687, L95
Pinnington, E. H., Berends, R. W., & Lumsden, M. 1995, J. Phys. B, 28, 2095
Quinet, P., Palmeri, P., Biémont, E., et al. 2006, A&A, 448, 1207
Rapol, U. D., Krishna, A., & Natarajan, V. 2003, EPJ D, 23, 185
Rehse, S. J., Li, R., Scholl, T. J., et al. 2006, Can. J. Phys., 84, 723
Roederer, I. U., Preston, G. W., Thompson, I. B., Shectman, S. A., & Sneden, C. 2014, ApJ, 784, 158
Rosman, K. J. R., & Taylor, P. D. P. 1998, Pure & Appl. Chem., 70, 217
Ross, J. E., & Aller, L. H. 1970, Proc. Nat. Acad. Sci., 66, 983
Ross, J. E., & Aller, L. H. 1972, Sol. Phys., 25, 30
Ross, J. E., & Aller, L. H. 1976, Science, 191, 1223
Rutten, R. J. 1978, Sol. Phys., 56, 237
Rutten, R. J., & Kostik, R. I. 1982, A&A, 115, 104
Scott, P., Grevesse, N., Asplund, M., et al. 2014a, A&A, 573, A25 (Paper I)
Scott, P., Asplund, M., Grevesse, N., Bergemann, M., & Sauval, A. J. 2014b, A&A, 573, A26 (Paper II)
Shi, J. R., Gehren, T., Zeng, J. L., Mashonkina, L., & Zhao, G. 2014, ApJ, 782, 80
Simsarian, J. E., Orozco, L. A., Sprouse, G. D., & Zhao, W. Z. 1998, Phys. Rev. A, 57, 2448
Sneden, C., & Crocker, D. A. 1988, ApJ, 335, 406
Sneden, C., Cowan, J. J., Lawler, J. E., et al. 2003, ApJ, 591, 936
Sneden, C., Cowan, J. J., & Gallino, R. 2008, ARA&A, 46, 241
Sneden, C., Lawler, J. E., Cowan, J., Ivans, I., & Den Hartog, E. 2009, ApJS, 182, 80
Takeda, Y., Hashimoto, O., Taguchi, H., et al. 2005, PASJ, 57, 751
Trapp, S., Marx, G., Tommaseo, G., et al. 2000, Hyperfine Interactions, 127, 57
Truran, J. W. 1981, A&A, 97, 391
Unsöld, A. 1955, Physik der Sternatmospharen, mit besonderer Berucksichtigung der Sonne, 2nd edn. (Berlin: Springer)
van Hove, M., Borghs, G., de Bisschop, P., & Silverans, R. E. 1982, J. Phys. B, 15, 1805
van Hove, M., Borghs, G., de Bisschop, P., & Silverans, R. E. 1985, Z. Phys. A, 321, 215
Veer, W. E. V. D., Blonk, D. P. V. D., Dönszelmann, A., & Snoek, C. 1990, A&A, 231, 277
Velichko, A. B., Mashonkina, L. I., & Nilsson, H. 2010, Astron. Lett., 36, 664
Velichko, A. B., Mashonkina, L. I., & Nilsson, H. 2011, Astron. Lett., 37, 440
Villemoes, P., Arnesen, A., Heijkenskjöld, F., & Wännström, A. 1993, J. Phys. B, 26, 4289
Vitas, N., Vince, I., Lugaro, M., et al. 2008, MNRAS, 384, 370
Volz, U., & Schmoranzer, H. 1996, Phys. Scr., 65, 48
Wännström, A., Vogel, O., Arnesen, A., & Hallin, R. 1988, Phys. Scr., 38, 564
Wanajo, S. 2013, ApJ, 770, L22
Wendt, K., Ahmad, S. A., Buchinger, F., et al. 1984, Z. Phys. A, 318, 125
Wessel, G., & Lew, H. 1953, Phys. Rev., 92, 641
Whaling, W., & Brault, J. W. 1988, Phys. Scr., 38, 707
Whaling, W., Hannaford, P., Lowe, R. M., Biémont, E., & Grevesse, N. 1984, J. Quant. Spectr. Rad. Transf., 32, 69
Wickliffe, M. E., Salih, S., & Lawler, J. E. 1994, J. Quant. Spectr. Rad. Transf., 51, 545
Xu, H. L., Sun, Z. W., Dai, Z. W., et al. 2006, A&A, 452, 357
Xu, H. L., Svanberg, S., Quinet, P., Palmeri, P., & Biémont, E. 2007, J. Quant. Spectr. Rad. Transf., 104, 52
Ye, J., Swartz, S., Jungner, P., & Hall, J. L. 1996, Opt. Lett., 21, 1280
Youssef, N. H. 1986, A&A, 164, 395
Youssef, N. H., & Khalil, N. M. 1988, A&A, 203, 378
Youssef, N. H., Dönszelmann, A., & Grevesse, N. 1990, A&A, 239, 367

Table 1. Lines retained in this analysis: atomic and solar data, line weightings, LTE abundance results for the 5 models used in this analysis, NLTE corrections to the LTE result (when available), and the corresponding 3D+NLTE abundance result.

λ (nm)	E_{exc} (eV)	$\log gf$	gf Ref.	W_λ (pm)	Wt.	3D	⟨3D⟩	HM	MARCS	MISS	Δ_{NLTE} (3D)	3D NLTE
						Cu I						
510.5541	1.390	−1.516	1	9.300	1	4.152	4.135	4.217	4.087	4.141	+0.020	4.172
521.8201	3.820	+0.264	1	5.250	1	4.214	4.185	4.228	4.125	4.207	+0.020	4.234
522.0070	3.820	−0.616	1	1.450	1	4.220	4.223	4.264	4.182	4.251	+0.010	4.230
793.3130	3.790	−0.372	2	2.800	1	4.187	4.176	4.216	4.133	4.196	−0.050	4.137
809.2634	3.820	−0.045	2	4.200	1	4.169	4.142	4.182	4.094	4.157	−0.050	4.119
						Zn I						
472.2159	4.030	−0.380	3	6.800	1	4.687	4.580	4.603	4.511	4.602	−0.032	4.655
481.0534	4.080	−0.160	3	7.500	1	4.649	4.539	4.560	4.466	4.559	−0.039	4.610
636.2347	5.800	+0.140	4	2.150	1	4.535	4.519	4.524	4.469	4.545	−0.014	4.521
1105.4280	5.800	−0.330	4	1.400	1	4.485	4.475	4.481	4.435	4.500	−0.018	4.467
1305.3650	6.650	+0.320	4	1.900	2	4.548	4.549	4.558	4.507	4.575	−0.007	4.541
						Ga I						
417.2053	0.100	−0.337	5	5.220	1	3.023	3.003	3.085	2.956	3.019		
						Ge I						
326.9489	0.890	−1.080	6	4.350	1	3.634	3.547	3.624	3.511	3.566		
						Rb I						
780.0268	0.000	+0.144	7	0.670	1	2.530	2.574	2.627	2.537	2.595		
794.7603	0.000	−0.164	7	0.270	1	2.417	2.462	2.514	2.425	2.484		
						Sr I						
460.7340	0.000	+0.283	8	4.450	2	2.698	2.688	2.771	2.644	2.705	+0.146	2.844
707.0100	1.830	−0.030	9	0.135	2	2.680	2.719	2.774	2.680	2.743	+0.084	2.764
						Sr II						
1003.6670	1.810	−1.202	10	6.650	2	2.963	2.876	2.887	2.831	2.886	−0.091	2.872
1032.7360	1.840	−0.248	10	14.860	3	3.078	2.982	2.995	2.918	2.986	−0.208	2.870
1091.4880	1.810	−0.478	10	12.360	1	2.936	2.829	2.843	2.772	2.834	−0.195	2.741
						Y II						
412.4909	0.410	−1.500	11	1.880	1	2.179	2.168	2.203	2.153	2.202		
439.8015	0.130	−1.000	11	4.600	1	2.116	2.065	2.101	2.032	2.092		
490.0124	1.030	−0.101	12	5.550	2	2.291	2.200	2.228	2.154	2.223		
508.7425	1.080	−0.170	11	4.700	1	2.156	2.091	2.116	2.050	2.116		
511.9119	0.990	−1.360	11	1.370	1	2.326	2.318	2.345	2.298	2.349		
520.0414	0.990	−0.570	11	3.500	1	2.149	2.113	2.139	2.081	2.142		
528.9821	1.030	−1.850	11	0.370	1	2.205	2.204	2.229	2.185	2.237		
547.3385	1.740	−0.954	13	0.670	1	2.248	2.244	2.265	2.223	2.276		
572.8876	1.840	−1.054	13	0.330	1	2.092	2.089	2.110	2.070	2.121		
						Zr I						
424.1706	0.650	+0.140	14	0.270	1	2.247	2.346	2.428	2.320	2.369		
454.2234	0.630	−0.310	14	0.430	1	2.855	2.955	3.038	2.927	2.977		
468.7805	0.730	+0.550	14	0.850	1	2.410	2.498	2.579	2.469	2.519		
480.9477	1.580	+0.160	14	0.145	1	2.828	2.894	2.966	2.862	2.920		
481.5637	0.600	−0.030	14	0.275	1	2.311	2.416	2.499	2.389	2.437		
538.5128	0.520	−0.710	14	0.185	1	2.678	2.793	2.877	2.766	2.811		
644.5720	1.000	−0.830	14	0.090	1	2.892	2.994	3.075	2.963	3.012		
710.2890	0.650	−0.840	14	0.060	1	2.318	2.442	2.525	2.416	2.456		
						Zr II						
350.5666	0.164	−0.375	15	5.350	1	2.666	2.527	2.564	2.491	2.551		
360.7369	1.236	−0.670	15	1.250	1	2.522	2.503	2.532	2.487	2.537		
367.1264	0.713	−0.590	15	3.150	1	2.480	2.449	2.483	2.429	2.481		
371.4777	0.527	−0.950	15	2.750	1	2.542	2.519	2.554	2.501	2.551		
402.4435	0.999	−1.130	16	1.350	1	2.659	2.650	2.682	2.638	2.684		

References. 1. Kock & Richter (1968), renormalised to lifetimes of Carlsson et al. (1989); 2. Meggers et al. (1961), via Bielski (1975); 3. Ref. 4, renormalised to lifetimes of Kerkhoff et al. (1980); 4. Biémont & Godefroid (1980a); 5. Cunningham & Link (1967); 6. Biémont et al. (1999); 7. mean of lifetimes from Simsarian et al. (1998) and Volz & Schmoranzer (1996) weighted according to uncertainties, via Morton (2000); 8. Migdalek & Baylis (1987); 9. Garcia & Campos (1988), normalised by them to other existing lifetimes 10. relative data of Gallagher (1967), normalised with the mean of (equal uncertainty) lifetimes from Kuske et al. (1978) and Pinnington et al. (1995); 11. Hannaford et al. (1982); 12. Ref. 11, renormalised with unweighted mean of lifetimes from Ref. 11 and Wännström et al. (1988); 13. Ref. 11, renormalised using un-weighted mean of lifetimes from Ref. 11, Wännström et al. (1988) and Biémont et al. (2011); 14. Biémont et al. (1981); 15. Log-scale mean of Refs. 14 and 16; 16. Ljung et al. (2006).

Table 1. continued.

λ (nm)	$E_{\rm exc}$ (eV)	log gf	gf Ref.	W_λ (pm)	Wt.	LTE Abundances					$\Delta_{\rm NLTE}$ (3D)	3D NLTE
						3D	⟨3D⟩	HM	MARCS	MISS		
403.4083	0.802	−1.530	15	0.790	1	2.594	2.590	2.624	2.579	2.624		
405.0320	0.713	−1.025	15	2.200	3	2.571	2.555	2.589	2.538	2.589		
420.8980	0.713	−0.485	15	4.400	2	2.627	2.569	2.602	2.536	2.599		
425.8041	0.559	−1.170	15	2.350	1	2.585	2.569	2.603	2.550	2.602		
444.2992	1.486	−0.375	15	2.200	1	2.608	2.590	2.618	2.567	2.624		
						Nb II						
319.4974[a]	0.326	+0.120	17		1	1.473		1.50				
321.5593[a]	0.439	−0.235	17		1	1.505		1.53				
371.7060[a]	1.694	+0.030	18		1	1.455		1.48				
374.0725[a]	1.619	−0.307	17		1	1.442		1.47				
						Mo I						
550.6496	1.335	+0.060	19	0.450	1	1.937	2.011	2.090	1.983	2.031		
553.3034	1.335	−0.069	19	0.270	1	1.824	1.907	1.988	1.877	1.928		
						Ru I						
343.6736	0.148	+0.150	20	1.000	1	1.572	1.653	1.749	1.632	1.670		
349.8945	0.000	+0.310	20	2.050	1	1.689	1.742	1.842	1.719	1.756		
374.2280	0.336	−0.180	20	0.740	1	1.849	1.935	2.028	1.915	1.955		
408.0600	0.812	−0.040	20	0.280	1	1.670	1.755	1.841	1.731	1.778		
455.4517	0.812	+0.070	20	0.550	1	1.819	1.898	1.985	1.874	1.918		
458.4443	1.002	−0.550	20	0.105	1	1.881	1.960	2.042	1.933	1.982		
						Rh I						
343.4889	0.000	+0.450	21	1.130	1	0.930	1.002	1.096	0.982	1.018		
369.2361	0.000	+0.150	21	0.655	1	0.853	0.948	1.037	0.928	0.966		
						Pd I						
324.2701	0.810	+0.070	22	2.400	1	1.533	1.528	1.616	1.504	1.547		
340.4581	0.810	+0.330	22	3.330	1	1.565	1.510	1.602	1.483	1.526		
						Ag I						
328.0681	0.000	−0.021	23	3.500	1	1.044	1.000	1.093	0.971	1.015		
338.2900	0.000	−0.333	23	2.230	1	0.869	0.893	0.986	0.870	0.911		
						Cd I						
508.5823	3.950	−0.144	24	0.073	1	1.766	1.760	1.792	1.728	1.793		
						Sn I						
380.1025	1.770	−0.620	25	0.120	1	2.016	2.061	2.130	2.036	2.088		
						Ba II						
455.4036	0.000	+0.172	26	18.200	1	2.236	2.208	2.241	2.150	2.226	−0.016	2.220
585.3688	0.600	−1.026	26	6.300	1	2.391	2.250	2.280	2.203	2.263	−0.080	2.311
649.6908	0.600	−0.407	27	9.960	1	2.372	2.244	2.271	2.185	2.249	−0.147	2.225
						W I						
400.8750[b]	0.360	−0.446	28	0.350	1	0.788		0.976				
484.3846[b]	0.410	−1.471	29	0.035	1	0.880		1.081				
						Os I						
330.1559	0.000	−0.743	30	0.960	1	1.405	1.413	1.496	1.396	1.437		
						Ir I						
322.0775	0.350	−0.536	31	0.975	1	1.418	1.398	1.455	1.381	1.429		
						Au I						
312.2784	1.140	−0.950	32	0.290	1	0.908	0.891	0.925	0.878	0.927		
						Pb I						
368.3480	0.970	−0.524	33	0.855	1	1.796	1.854	1.934	1.831	1.876	+0.120	1.916
						Th II						
401.9130	0.000	−0.228	34	0.314	1	0.018	0.021	0.059	0.012	0.055	+0.010	0.028

Notes. [a] 3D correction applied to HM results of Nilsson et al. (2010). [b] 3D correction and gf update applied to HM results of Holweger & Werner (1974).

References. 17. Nilsson & Ivarsson (2008); 18. Nilsson et al. (2010); 19. Whaling & Brault (1988); 20. Wickliffe et al. (1994); 21. Kwiatkowski et al. (1982); 22. Xu et al. (2006); 23. Total doublet strength from lifetime of Carlsson et al. (1990), with the relative contribution of each line given by theoretical data of Civiš et al. (2010); 24. Veer et al. (1990); 25. Lotrian et al. (1976); 26. Kurz et al. (2008); 27. Davidson et al. (1992); 28. log-scale mean of Ref. 29 and Kling & Kock (1999); 29. den Hartog et al. (1987); 30. Ivarsson et al. (2003); 31. Gough et al. (1983), renormalised using the uncertainty-weighted mean of lifetimes from Gough et al. and Xu et al. (2007); 32. Hannaford et al. (1981); 33. Biémont et al. (2000); 34. Nilsson et al. (2002).

Table 2. HFS and isotopic splitting data for the lines retained in this analysis.

λ (nm)	Iso.	Lower level J	A (MHz)	B (MHz)	HFS Ref.	Upper level J	A (MHz)	B (MHz)	HFS Ref.
Cu I : 69.2% ^{63}Cu ($I = \frac{3}{2}$), 30.8% ^{65}Cu ($I = \frac{3}{2}$)								
Isotopic separation for 510.6 nm from Ref. 1								
510.5541	^{63}Cu	5/2	749.781	188.270	1	3/2	194.595	−28.480	2
510.5560	^{65}Cu	5/2	804.043	172.980	1	3/2	208.464	−26.356	2
521.8201	^{63}Cu	3/2	194.595	−28.480	2	5/2			
521.8201	^{65}Cu	3/2	208.464	−26.356	2	5/2			
522.0070	^{63}Cu	3/2	194.595	−28.480	2	3/2			
522.0070	^{65}Cu	3/2	208.464	−26.356	2	3/2			
Rb I : 72.2% ^{85}Rb ($I = \frac{5}{2}$), 27.8% ^{87}Rb ($I = \frac{3}{2}$)								
780.0268	^{85}Rb	1/2	1011.911		3	3/2	25.009	25.039	4
780.0268	^{87}Rb	1/2	3417.341		5	3/2	84.718	12.497	6
794.7603	^{85}Rb	1/2	1011.911		3	1/2	120.720		7
794.7603	^{87}Rb	1/2	3417.341		5	1/2	406.200		7
Y II : 100% ^{89}Y ($I = \frac{1}{2}$)								
412.4909	^{89}Y	2	15.500		8	3	−64.400		8
439.8015	^{89}Y	2	−222.900		8	1	−108.000		8
490.0124	^{89}Y	3				2	−22.800		8
508.7425	^{89}Y	4				4	−29.000		8
511.9119	^{89}Y	2	−149.940		9	3	−64.400		8
520.0414	^{89}Y	2	−149.940		9	2	−79.300		8
528.9821	^{89}Y	3				2	−79.300		8
547.3385	^{89}Y	1	46.560		10	2	−67.000		8
572.8876	^{89}Y	2	−26.400		10	2	−67.000		8
Nb II : 100% ^{93}Nb ($I = \frac{9}{2}$)								
319.4974	^{93}Nb	2	513.245		11	3	614.275		11
321.5593	^{93}Nb	4	989.915		11	4	358.552		11
371.7060	^{93}Nb	4	76.147		11	4	160.389		11
374.0725	^{93}Nb	3	554.616		11	3	220.347		11
Rh I : 100% ^{103}Rh ($I = \frac{1}{2}$)								
343.4889	^{103}Rh	9/2	−175.574		12	11/2			
369.2361	^{103}Rh	9/2	−175.574		12	7/2			
Ag I : 51.8% ^{107}Ag ($I = \frac{1}{2}$), 48.2% ^{109}Ag ($I = \frac{1}{2}$)								
Isotopic separations calculated from the data of Crawford et al. (1949) and Jackson &								
Kuhn (1937), but using component identifications of Brix et al. (1951) and Ref. 13								
328.06810	^{107}Ag	1/2	−1712.560		13	3/2	−31.700		14
328.06827	^{109}Ag	1/2	−1976.940		13	3/2	−36.700		14
338.29000	^{107}Ag	1/2	−1712.560		13	1/2	−175.400		14
338.29018	^{109}Ag	1/2	−1976.940		13	1/2	−201.600		14

References. 1. Fischer et al. (1967); 2. Hannaford & McDonald (1978); 3. Nez et al. (1993); 4. Rapol et al. (2003); 5. Bize et al. (1999); 6. Ye et al. (1996); 7. Beacham & Andrew (1971); 8. Wännström et al. (1988); 9. Beck (1992); 10. Dinneen et al. (1991); 11. Nilsson & Ivarsson (2008); 12. Chan et al. (1968); 13. Wessel & Lew (1953); 14. Carlsson et al. (1990).

Table 2. continued.

λ (nm)	Iso.	Lower level				Upper level			
		J	*A* (MHz)	*B* (MHz)	HFS Ref.	*J*	*A* (MHz)	*B* (MHz)	HFS Ref.
Ba II : 0.1% ^{130}Ba ($I = 0$), 0.1% ^{132}Ba ($I = 0$), 2.4% ^{134}Ba ($I = 0$),									
6.6% ^{135}Ba ($I = \frac{3}{2}$), 7.9% ^{136}Ba ($I = 0$), 11.2% ^{137}Ba ($I = \frac{3}{2}$), 71.7% ^{138}Ba ($I = 0$)									
Isotopic separations from Wendt et al. (1984; 455.4 nm), van Hove et al. (1982; 585.4 nm), and Ref. 17 (649.7 nm)									
455.40334	^{130}Ba	1/2	0.000	0.000	N	3/2	0.000	0.000	N
455.40335	^{135}Ba	1/2	3591.670		15	3/2	113.000	59.000	16
455.40340	^{132}Ba	1/2	0.000	0.000	N	3/2	0.000	0.000	N
455.40341	^{137}Ba	1/2	4018.871		15	3/2	127.200	92.500	16
455.40344	^{134}Ba	1/2	0.000	0.000	N	3/2	0.000	0.000	N
455.40347	^{136}Ba	1/2	0.000	0.000	N	3/2	0.000	0.000	N
455.40360	^{138}Ba	1/2	0.000	0.000	N	3/2	0.000	0.000	N
585.36879	^{137}Ba	3/2	189.730	44.541	17	3/2	127.200	92.500	16
585.36880	^{138}Ba	3/2	0.000	0.000	N	3/2	0.000	0.000	N
585.36889	^{136}Ba	3/2	0.000	0.000	N	3/2	0.000	0.000	N
585.36891	^{135}Ba	3/2	169.590	28.953	17	3/2	113.000	59.000	16
585.36902	^{134}Ba	3/2	0.000	0.000	N	3/2	0.000	0.000	N
585.36914	^{132}Ba	3/2	0.000	0.000	N	3/2	0.000	0.000	N
585.36927	^{130}Ba	3/2	0.000	0.000	N	3/2	0.000	0.000	N
649.69078	^{137}Ba	3/2	189.730	44.541	17	1/2	743.700		16
649.69080	^{138}Ba	3/2	0.000	0.000	N	1/2	0.000	0.000	N
649.69090	^{136}Ba	3/2	0.000	0.000	N	1/2	0.000	0.000	N
649.69091	^{135}Ba	3/2	169.590	28.953	17	1/2	664.600		16
649.69105	^{134}Ba	3/2	0.000	0.000	N	1/2	0.000	0.000	N

References. 15. Trapp et al. (2000); 16. Villemoes et al. (1993); 17. van Hove et al. (1985); N) no HFS because $J = 0$ or $I = 0$.

Table 3. Adopted ionisation energies χ_{ion} and partition functions $U(T)$ for the relevant ionisation stages of the heavy elements.

Species	E_{ion} (eV)	$U(T)$				Species	E_{ion} (eV)	$U(T)$			
		3000 K	5000 K	8000 K	12 000 K			3000 K	5000 K	8000 K	12 000 K
Cu I	7.726	2.04	2.34	3.23	5.63	Pr II	10.600	55.98	138.35	318.42	585.87
Cu II	20.290	1.01	1.03	1.33	2.23	Nd I	5.525	30.35	92.55	322.69	828.45
Zn I	9.394	1.00	1.01	1.01	1.35	Nd II	10.700	49.58	120.48	315.29	705.33
Zn II	17.960	2.00	2.00	2.00	2.02	Sm I	5.644	18.22	38.24	108.47	299.28
Ga I	5.999	4.70	5.12	5.65	8.15	Sm II	11.100	31.27	59.16	120.02	243.16
Ga II	20.520	1.00	1.00	1.00	1.03	Eu I	5.670	8.16	10.97	28.31	103.98
Ge I	7.899	6.03	7.61	9.01	12.29	Eu II	11.240	12.49	15.87	23.96	42.00
Ge II	15.940	3.71	4.41	4.90	5.27	Gd I	6.150	34.56	59.41	135.19	318.79
Rb I	4.177	1.99	2.25	4.26	11.85	Gd II	12.100	48.42	83.38	146.39	249.09
Rb II	27.290	1.00	1.00	1.00	1.00	Tb I	5.864	90.06	165.84	348.95	703.54
Sr I	5.695	1.01	1.24	3.01	19.84	Tb II	11.500	53.44	102.16	181.93	293.33
Sr II	11.030	2.00	2.15	2.78	4.26	Dy I	5.939	20.94	41.18	137.28	441.21
Y I	6.217	8.84	11.76	20.43	37.35	Dy II	11.700	33.55	54.46	127.72	320.92
Y II	12.220	10.94	15.79	22.54	31.80	Ho I	6.022	18.57	34.40	96.02	261.06
Zr I	6.634	19.93	32.50	55.44	89.33	Ho II	11.800	31.09	49.39	131.82	424.08
Zr II	13.130	29.14	45.59	67.79	96.11	Er I	6.108	16.14	32.36	102.58	318.00
Nb I	6.579	34.95	52.93	93.16	192.18	Er II	11.900	26.97	42.14	90.26	204.14
Nb II	14.320	26.20	43.07	71.77	114.13	Tm I	6.184	7.95	10.60	28.30	106.31
Mo I	7.092	7.12	9.05	19.54	56.94	Tm II	12.100	15.42	17.79	31.30	76.72
Mo II	16.160	6.03	7.72	15.75	38.08	Yb I	6.254	0.94	1.02	2.33	9.85
Ru I	7.361	22.45	34.02	56.98	97.48	Yb II	12.180	2.01	2.00	3.04	8.23
Ru II	16.760	15.99	23.97	36.74	58.12	Lu I	5.426	6.69	8.70	14.05	29.32
Rh I	7.459	18.66	26.51	38.86	58.73	Lu II	13.900	1.02	1.40	2.79	5.91
Rh II	18.080	11.77	15.50	21.00	30.21	Hf I	6.825	9.07	14.60	27.72	58.17
Pd I	8.337	1.53	2.94	5.74	10.30	Hf II	14.900	6.91	12.63	22.14	38.13
Pd II	19.430	6.68	7.51	8.50	10.52	W I	7.864	6.25	12.72	28.41	68.89
Ag I	7.576	1.96	1.96	2.05	3.42	W II	17.700	6.95	13.84	29.34	60.05
Ag II	21.490	0.98	1.00	1.03	1.16	Os I	8.438	12.99	20.01	36.56	71.82
In I	5.786	3.46	4.23	5.42	12.28	Os II	18.500	12.12	18.01	27.13	40.49
In II	18.870	1.00	1.00	1.01	1.05	Ir I	8.967	14.50	21.10	33.66	57.06
Sn I	7.344	3.36	5.14	7.07	9.33	Ir II	17.000	16.46	22.92	34.68	53.96
Sn II	14.630	2.57	3.13	3.83	4.42	Au I	9.226	2.10	2.46	3.27	4.72
Ba I	5.212	1.22	2.55	8.35	29.87	Au II	20.500	0.81	1.12	1.80	3.17
Ba II	10.000	2.78	4.17	5.97	7.95	Tl I	6.108	2.00	2.29	2.95	5.40
La I	5.577	14.29	27.04	58.19	126.50	Tl II	20.430	1.00	1.00	1.01	1.02
La II	11.100	20.23	29.25	42.52	62.91	Pb I	7.417	1.11	1.54	2.70	7.13
Ce I	5.539	75.34	190.04	471.79	998.10	Pb II	15.030	2.00	2.10	2.33	2.75
Ce II	10.800	81.74	189.36	369.03	604.79	Th I	6.307	11.19	27.29	81.41	221.47
Pr I	5.473	37.48	115.76	333.07	717.89	Th II	11.900	14.73	35.99	88.25	187.33